ISOTOPE SHIFT OF THE $K_{\alpha 1}$ X-RAY IN URANIUM

Thesis by

Richard Taber Brockmeier

In Partial Fulfillment of the Requirements

For the Degree of

Doctor of Philosophy

California Institute of Technology

Pasadena, California

1965

ACKNOWLEDGEMENTS

The author would like to express his gratitude to Dr. Felix Boehm for his close interest throughout all phases of this project. The author feels it has been a privilege to have had the opportunity of working and learning under his guidance.

The author would also like to express his thanks to Dr. Eastman Hatch who first conceived of the possibility of performing this experiment and who obtained and helped prepare the isotope samples.

Many other people have contributed to the success of this experiment. The author wishes to thank: Mr. H.E. Henrikson, the designer of the Caltech spectrometer. The success of the project owes much to his knowledge and experience. Dr. J.W.M. DuMond for his interest and helpful suggestions. Dr. Z.L. Szymanski and Dr. H.D. Zeh for valuable discussions. Dr. Milton Clauser for his generous loan of the set of thermo-micrometers which proved so invaluable. Mr. R. Chesler and Mr. L. Varnell for their help in the experimental design and assistance in the data collection during the early stages of the experiment.

The author gratefully acknowledges financial aid from the California Institute of Technology, the U.S. Atomic Energy Commission, the Danforth Foundation, and the Woodrow Wilson Foundation.

Finally, the author wishes to thank his wife, Helen, for her constant cooperation and encouragement.

ABSTRACT

The first experimental evidence of the isotopic shift of electronic K x-rays has been found. A two-meter focal length curved-crystal diffraction spectrometer was used to measure the wavelengths of fluorescent $K_{\alpha 1}$ x-rays from isotopically pure U^{233} and U^{238} samples. The difference in wavelengths was found to be 0.00228 ± 0.00022 x-units. This corresponds to a 1.8 ± 0.2 eV energy difference, the U^{233} x-ray being higher in energy. The result is discussed in terms of 1) the pure volume effect, 2) the even-odd staggering contributions, 3) the change of intrinsic quadrupole moments, and 4) the nuclear compressibility factor. Good agreement between the experimental result and theory is obtained by considering either the pure volume effect, or by considering the contributions of all four effects choosing the parameter for the nuclear compressibility somewhat higher than inferred from the optical isotope shift measurements.

TABLE OF CONTENTS

LIST OF FIGURES

I. INTRODUCTION

With the high-energy resolution available in optical spectroscopy, a hyperfine structure and an isotope shift have been observed in the optical spectra of many elements. The hyperfine structure has been well understood as an interaction between the orbital electrons and the nucleus with a magnetic moment μ and an electric quadrupole moment Q. In a simple view of the isotope shift, the shift can be divided into two types: 1) the mass-dependent effect, and 2) the volume dependent effect. In the first type, the energy of the shifted level is changed because the reduced mass of the electron is raised with the addition of a neutron to the nucleus. The size of the mass-dependent shift decreases with increasing Z and becomes negligible in optical spectra for $M > 140$. In contrast, the volume dependent shift <u>increases</u> with Z and for $M > 100$ is the dominant cause of the isotope shift. This thesis will be concerned with the volume-dependent isotope shift.

The volume-dependent isotope shift represents changes in the energy of an atomic electron as neutrons are added to the nucleus of an element. The addition of neutrons to a nucleus expands the nuclear charge distribution experienced by an electron whose wave function penetrates into the nucleus resulting in a decrease of the binding energy of that electron. Since only $s_{\frac{1}{2}}$ or $p_{\frac{1}{2}}$ electrons have wave functions which overlap with the nuclear volume to any appreciable extent, the levels of these electrons are the only ones which have been found to exhibit a volume-dependent isotope shift.

The nuclear volume-dependent isotope shift of optical spectral lines has long been a very useful means for studying the changes in the nuclear size or shape for different isotopes of elements beginning with M ≳ 100 and on up to the end of the periodical chart. The first observation of the volume-dependent isotope shift was apparently made by Merton in 1919[1]. Later, in the early 1930's, theoretical estimates of the expected shifts were calculated by Bartlett[2], Pauli and Peierls[3], Racah[4], Rosenthal and Breit[5], and Breit[6].

Following this work, many observations of the volume-dependent shift of optical spectral lines were carried out and the theory was refined using more modern theoretical techniques. Reviews of some of the experimental measurements have been compiled by Mack and Arroe[7] and by Brix and Kopfermann[8], and two recent reviews of the theory have been given by Breit[9] and by Kopfermann[10].

From the large number of observations of the optical isotope shift and the theoretical interpretations which have been advanced to explain these data, several general features of the shift have emerged in which there is a partial failure to fully understand the shift. Three such features are:

1. the anomaly of the even-odd staggering,
2. the theoretical overestimate of the magnitude of the shift, (in most cases by about 40%), and
3. discrepancies in the shift for isotopes with N ≈ 90[11].

Part of the difficulty resides in the problem of not being able

to separate the roles that atomic and nuclear effects play in the shift. Optical transitions involve outer electrons. Hence, shielding corrections for optical isotope shifts are large. If it were possible to detect a shift in energy of one of the inner electrons, a more reliable comparison with theory could be made because of the availability of better electron wave functions. Thus, experimental observations of x-ray isotope shifts would contribute to the understanding of the deficiencies of the present isotope shift theory.

Many efforts have been made to observe either hyperfine structure or isotope shifts in atomic x-rays. Richtmyer and Barnes[12] investigated the K_α lines of W, while Williams[13] measured some lines of the U L series. Frilley, Gokhale, and Valadarès[14] attempted to observe hyperfine structure in the x-rays of several other elements. All these gave negative results, apparently due to lack of resolution. Rogosa and Schwarz[15] attempted to observe the isotope shift in the K_α x-rays of Mo and in some of the L x-rays of U, but no effect was detected. A later calculation by Wertheim and Igo[16] showed that the isotope shifts of the $1s_{\frac{1}{2}}$, $2s_{\frac{1}{2}}$ and $2p_{\frac{1}{2}}$ electron states in Mo and U were too small to be observable with the resolution available to Rogosa and Schwarz. However, an extrapolation of this same calculation showed that the $K_{\alpha 1}$ line (a $2p_{3/2}$ to $1s_{1/2}$ transition) might show a shift which is of the same order of magnitude as some of the error limits presently assigned to some of the more accurate measurements made with the bent-crystal

spectrometer. It is believed that this was first recognized by Hatch[17].

It is the aim of this thesis project to investigate whether the California Institute of Technology two meter bent-crystal spectrometer can be used to study the isotope shift of x-rays. To accomplish this, the goal was set to select a favorable initial pair of isotopes in which the expected shift is large and attempt to detect and measure the size of this shift. From the results of such an experiment, it should be possible to predict the usefulness of the bent-crystal spectrometer in measuring additional isotope shifts.

II. SELECTION OF THE INITIAL CASE

A. Resolution of the Bent-Crystal Spectrometer

Measurements on a crystal diffraction spectrometer are proportional to the wavelength of the radiation. It is therefore appropriate to express spectrometer capabilities and results in x-units, a wavelength scale introduced by Siegbahn in 1919 and at that time based on the grating constant of calcite. The x-unit scale is now standardized by taking the $K_{\alpha 1}$ x-ray line of tungsten to be 208.5770 x-units[18]. The relationship of x-units to energy then is[18]:

$$\lambda \text{ (x-units)} = \frac{12372.42\ (\pm.13)}{E(\text{keV})} \ . \qquad (1)$$

The resolution of the bent-crystal spectrometer expressed in x-units is a constant independent of wavelength. It depends on the following factors: 1) the natural line-width, 2) the size of the sample, 3) the cylindrical aberration effect, and 4) the properties of the crystal such as the non-uniform bending, the mosaic, and lineage defects. The resolution of a line can be improved by a factor of n if it can be measured in n-th order. Owing to the reduced reflectivity in higher orders, this requires that counting rates be sufficiently high compared to the background.

For the two-meter focal length bent-crystal spectrometer at Caltech, the following numbers serve as an illustration of the geometrical conditions. For a 10-mil wide sample, the observed line width is primarily due to the sample width. The line-width decreases

with the sample diameter. Broadening effects due to non-uniform crystal bending and crystal defects become comparable to the sample broadening for 3-mil samples. Generally a compromise is chosen between 1) a high counting rate by means of a large sample and thus a broad line, or 2) a narrow line by means of a small sample and thus a lower counting rate.

B. The Line-Width

The natural line-width of gamma rays is negligible compared to the mentioned instrumental resolution. For x-rays, however, the natural line-width becomes comparable to the instrumental width. It is of interest, therefore, to recall the natural line-width of K x-rays as a function of Z. The literature values[19] of the measured natural line-widths of K x-rays expressed in x-units are presented in Fig. 1. The instrumental width for the 10-mil diameter samples used in this experiment is indicated by a horizontal line. It is evident that for low-Z atoms, the natural line-width is comparable to the instrumental width. For higher-Z atoms, the natural width is likely to give only a small contribution to the observed width.

Because the instrumental line-width expressed in x-units is a constant for all wavelengths, the resolution in energy units becomes poorer with increasing energy. A differentiation of Eq. (1) shows:

$$\Delta \lambda \text{ (x-units)} = \frac{12.37 \times 10^6}{E^2} \Delta E(\text{eV}) \ . \qquad (2)$$

If the variable E in this result is replaced with the Z^2 energy

dependence for K x-rays from Moseley's Law, one sees that the resolution of K x-rays becomes poorer with increasing Z by a factor of Z^4. This would seem to strongly favor looking for the shift in lower-Z elements.

C. Wertheim's Result and the Initial Selection

Although the resolution of the spectrometer for K x-rays decreases as Z^4, one must also check the magnitude of the isotope shift as a function of Z. A log plot of the results from Wertheim's first-order perturbation-theory calculations of the shift of the $1s_{\frac{1}{2}}$ electron for three elements is[16] displayed in Fig. 2. It has a slope of approximately Z^6 thus favoring high-Z elements. Evidently, the ratio of the magnitude of the isotope shift to instrumental resolution increases with increasing Z. This points to a high-Z case as being the best initial choice. Although resolution is poorer for high-Z, the Z dependence of the isotope shift is an overcompensating factor.

Thus, the search narrows down to the top of the periodic chart. For the initial case, the pair of isotopes should not be strongly radioactive in order to minimize background problems. In addition, the Δ A between the isotopes should be as large as possible thereby increasing the chances of detecting the shift. These requirements lead to the selection of U^{238} and U^{233}.

III. THEORETICAL CALCULATION OF THE SHIFT

A. Introduction

The calculation of the isotope shift presented here is based on a method Wertheim and Igo[16] used for the calculation of the isotope shift of the $L_{\beta 1}$ and $L_{\alpha 1}$ x-ray lines of U and the $K_{\alpha 1}$ line of Mo. The calculation is extended to include the isotope shift of the $K_{\alpha 1}$ x-ray of Uranium.

In the Wertheim calculation, the isotope shift is calculated with a simplifying top-slice model of the nucleus. In the top-slice model, all the charge of the nucleus resides on the surface. A correction to the top-slice result to account for the distortion of the wavefunction because of the finite size of the nucleus is given by Wertheim. Two corrections due to screening are then applied. Because of screening from the other electrons, there is a reduction in the probability density of the $1s_{\frac{1}{2}}$ electron being at the nucleus. This first correction has the effect of reducing the size of the shift. The second screening correction enters as a result of the shifts in energy of the other electrons which occur when they experience a change in screening as the $1s_{\frac{1}{2}}$ electron is removed or replaced. Because a top-slice potential has been used for the nucleus, a correction for more general charge distributions is given, and in particular for a uniform charge distribution.

B. First Order Perturbation Calculation

The first step in the calculation is a first order perturba-

tion treatment for a change in term energy δE^0_{TERM} from a point nucleus to a top-slice nucleus of radius a:

$$\delta E^0_{TERM} = (\psi_0, \delta V \psi_0) \tag{3}$$

where ψ_0 is the Coulomb-Dirac wavefunction. The difference in nuclear potential of the point and top-slice nucleus, δV, is non-zero only within the nucleus:

$$\begin{aligned} \delta V &= \frac{\gamma}{r} - \frac{\gamma}{R} \qquad r < a \\ \delta V &= 0 \qquad\qquad r > a \end{aligned} \tag{4}$$

where r is the radial distance in the $\hbar/mc$ units and $\gamma = Z\alpha$, the product of atomic number and the fine structure constant. This change in term energy δE^0_{TERM} is differentiated with respect to the nuclear radius which, as neutrons are added, is assumed to increase according to:

$$\frac{a\hbar}{mc} = R = R_0 A^{1/3} \tag{5}$$

from the liquid drop model where $R_0 = 1.2 \times 10^{-13}$ cm and A is the mass number. The isotope shift ΔE (unit mc^2) becomes:

$$\Delta E = \frac{\Delta \left[\int_0^a (F_0^2 + G_0^2)\, \delta V \, dr \right]}{\Delta a} \frac{\Delta a}{\Delta A} \Delta A \ , \tag{6}$$

where F_0 and G_0 are the small and large components of the Coulomb-Dirac wave function multiplied by r, and where the quantity in brackets is δE^0_{TERM} of Eq. (3). For the $1s_{\frac{1}{2}}$ electron, the wave function is:

$$\begin{pmatrix} F_0 \\ G_0 \end{pmatrix} = \sqrt{\frac{\gamma}{\Gamma(2\rho + 1)}} \; e^{-\gamma r} \; (2\gamma r)^{\rho} \begin{pmatrix} -\sqrt{1 - \rho} \\ +\sqrt{1 + \rho} \end{pmatrix} \qquad (7)$$

where $\rho = (1 - \gamma^2)^{1/2}$. For purposes of numerically evaluating Eq. (6), Wertheim shows that the setting of the exponential factor in the wave function equal to one introduces less than a 1 percent error and allows the isotope shift to be expressed as:

$$\Delta E = \frac{1}{3}\left[F_0^{\,2}(a) + G_0^{\,2}(a)\right] \frac{\gamma}{(2\rho + 1)} \; \frac{\Delta A}{A} \; . \qquad (8)$$

The results Wertheim obtained in this manner for a top-slice nucleus with Coulomb-Dirac wave functions and using the value $R_0 = 1.5 \times 10^{-13}$ cm are shown in Table I. From these results it is seen that the shift of

Table I

First order perturbation result for isotope shift

by Wertheim and Igo[16] in eV

element / electronic state	$_{92}U$	$_{82}Pb$	$_{42}Mo$
$1s_{\frac{1}{2}}$	1.2	0.50	0.012
$2s_{\frac{1}{2}}$	0.24	0.088	0.0016
$2p_{\frac{1}{2}}$	0.028	0.0068	0.00003

the $1s_{\frac{1}{2}}$ electron is by far the greatest and that the shift increases rapidly with increasing Z. Wertheim used an R_0 which is somewhat high. If the accepted value $R_0 = 1.2 \times 10^{-13}$ cm is used, the calculated values in Table I will be somewhat smaller. A recalculation of the shift of the $1s_{\frac{1}{2}}$ state in $_{92}U$ gives 0.88 eV instead of 1.2 eV.

C. Wave Function Distortion Correction

The first order perturbation result must be corrected for the distortion of the electron wave function by the extended nuclear charge distribution. The quantity δE_{TERM}, defined as the change in term energy due to the cutoff of the Coulomb field at the radius of a top-slice nucleus, is expressed in its exact form as:

$$\delta E_{TERM} = \frac{(\psi_0, \delta V\ \psi)}{(\psi_0,\ \psi)} \quad , \tag{9}$$

and is to be compared with δE^0_{TERM}, the quantity in brackets in Eq. (6). $\psi_0 = \begin{pmatrix} F_0 \\ G_0 \end{pmatrix}$ is the Dirac wave function in a pure Coulomb field (see Eq. (7)) and $\psi = \begin{pmatrix} F \\ G \end{pmatrix}$ is the exact Dirac wave function of the electron in the potential of a top-slice nucleus. The first-order perturbation result must be corrected for the error which distortion of the wave function introduces into Eq. (6). This Wertheim did by calculating an approximate expression for δE_{TERM} which was then tested for accuracy by numerical integration and found to be good within one or two percent. This approximate expression for δE_{TERM} was then compared with the expression for δE^0_{TERM}

used in Eq. (6). In this manner, the wave function distortion factor C_{WFD} was found to be:

$$C_{WFD} \equiv \frac{\delta E_{TERM}}{\delta E^{0}_{TERM}} \approx \frac{\rho(2\rho + 1)}{\rho + 2} \tag{10}$$

which for the case of uranium is 0.67.

D. Screening of the Valence Electron

The first of the two screening corrections is due to the screening of the valence electron wave function by all other electrons . In this thesis the term "valence electron" refers to the electron involved in the x-ray transition under consideration rather than one of the outer electrons generally referred to as the valence electron. Wertheim took the screening of the wave function correction to be:

$$C_{SWF} = \frac{(F^2_{FT}(a) + G^2_{FT}(a))}{(F^2_{COUL}(a) + G^2_{COUL}(a))} \tag{11}$$

the ratio of the probability density at the nuclear radius for the wave function of the valence electron in a Fermi-Thomas potential to that of a wave function in the Coulomb field. Using the phase amplitude method[20], Wertheim calculated C_{SWF} for the $2s_{\frac{1}{2}}$ and $2p_{\frac{1}{2}}$ electron in U by numerical integration of equations representing the perturbation of $\delta V(r)$ (where $\delta V(r)$ is the difference between the Fermi-Thomas and the Coulomb potential) on the unperturbed wave function in the Coulomb field. Results of:

$$C_{SWF}\ (2s_{\frac{1}{2}},\ Z = 92) = 0.90 \qquad (12a)$$

$$C_{SWF}\ (2p_{\frac{1}{2}},\ Z = 92) = 0.76 \qquad (12b)$$

$$C_{SWF}\ (1s_{\frac{1}{2}},\ Z = 42) = 0.98 \qquad (12c)$$

were found. Reitz[21], in connection with a calculation of the effects of screening on internal conversion and beta decay, calculated wave functions for the $1s_{\frac{1}{2}}$ and $2s_{\frac{1}{2}}$ electrons in a Fermi-Thomas field by direct numerical integration of the radial equations. Wertheim used this result for comparison with his calculation (Eq. (12)) by the phase-amplitude method and obtained agreement to within 2 percent.

For the case of the $1s_{\frac{1}{2}}$ electron, $C_{SWF}\ (1s_{\frac{1}{2}},\ Z)$ has been recently calculated[22] and the plot of $C_{SWF}\ (1s_{\frac{1}{2}},\ Z)$ as a function of Z shows that C_{SWF} increases with Z, until it levels off with $C_{SWF} \approx 0.99$. Thus we have for the case in which we are interested:

$$C_{SWF}\ (1s_{\frac{1}{2}},\ Z = 92) = 0.99. \qquad (12d)$$

E. Screening of the Non-Valence Electrons

The second screening correction involves the relative change in energy of the non-valence electrons due to the relative difference in the change of screening they experience when the valence electron makes its transition . An estimate using Eq. (12d) of the maximum contribution to the effect from the non-valence $1s_{\frac{1}{2}}$ electron due to

the other $1s_{\frac{1}{2}}$ electron if one ascribes all the shielding to this other $1s_{\frac{1}{2}}$ electron is 1 percent.

In the calculation of the contribution from the $2s_{\frac{1}{2}}$ electrons Wertheim notes that the isotope shift of the $2s_{\frac{1}{2}}$ electron shows the following approximate proportionality on γ and ρ:

$$\Delta E \propto \gamma \left(\frac{\gamma a}{E}\right)^{2\rho} \tag{13}$$

which gives for the fractional change in the isotope shift of a $2s_{\frac{1}{2}}$ electron for a change ΔZ in the shielding charge:

$$F(2s_{\frac{1}{2}}) \equiv \frac{\Delta [\Delta E]}{\Delta E} = \left[\frac{2\rho + 1}{Z} - \frac{2\gamma \ln(\gamma a/E)}{137\ \rho}\right] \Delta Z. \tag{14}$$

If it is assumed that the $2s_{\frac{1}{2}}$ electron sees a change in charge $\Delta Z = 1$ when a $1s_{\frac{1}{2}}$ electron is removed, then $F(2s_{\frac{1}{2}}) = 0.08$. Taking into account the relative magnitude of the $2s_{\frac{1}{2}}$ and $1s_{\frac{1}{2}}$ isotope shift (see Table I), it is calculated that the contribution to the isotope shift from the $2s_{\frac{1}{2}}$ electrons is at most 3 percent. At the same time, it can be seen that the contribution from the $2p_{\frac{1}{2}}$ electrons is negligible. The total possible contribution from the non-valence electrons adds up to 4 percent or $C_{SNV} = 0.96$.

F. Final Result for a Non-Deformed Nucleus of Uniform Charge

First order perturbation calculations have been performed by Breit[5] using a more general potential:

$$V - \left(\frac{-\gamma}{na}\right) \left[-\left(\frac{r}{a}\right)^{n} + n + 1\right] \tag{15}$$

with adjustable n. For $n = \infty$, the potential is a top-slice potential. With n = 2, it represents a uniform charge distribution, and as n becomes smaller, the charge distribution becomes more and more concentrated at the center of the nucleus. From Breit's general result, Wertheim shows that the correction factor for the shape of the nuclear potential C_{CD} is:

$$C_{CD} = \frac{[\Delta E]_n}{[\Delta E]_\infty} = \frac{n + 1}{2\rho + n + 1} \qquad (16)$$

C_{CD} has values 0.63, 0.67, and 0.70 for n = 1.5, 2.0, and 2.5, respectively.

Combining the corrections for the wave function distortion C_{WFD}, for the screening of the wave function C_{SWF}, for the contributions from the non-valence electrons C_{SNV}, and for a uniform charge distribution C_{CD}, and applying these to the first order perturbation result of 0.88 eV/Δ A for a spherical top-slice nucleus (Sec. B) we have for the $\Delta A = 5$ case of U-238 - U-233 the predicted values listed in Table II.

Table II

Result of the Isotope Shift Calculation for a Spherical Uniform Charge Nucleus of Radius $R = 1.2\ A^{1/3}_f$

$E(U^{238}) - E(U^{233}) = -1.8$ eV
$\lambda(U^{238}) - \lambda(U^{233}) = 0.0023$ x-units

G. Additional Considerations

The calculations performed thus far have not taken into consideration:

1) the mass effect,

2) even-odd staggering

3) deformation effects,

4) polarization effects, and

5) compressibility.

The mass effect, the major cause of the isotope shift observed at the lower end of the periodical chart, can be shown to cause a shift of less than 10^{-2} eV for uranium with $\Delta A = 5$. It is therefore safely negligible. However, the other considerations listed above can possibly give significant contributions to the shift and deserve study. However, their consideration will be deferred to Chapter VII where they will be discussed in connection with the experimental results for the isotope shift measurement.

IV. CONSTRUCTION OF THE EXPERIMENTAL SYSTEM TO DETECT THE SHIFT

A. General Considerations

The basic scheme for measuring the isotope shift is illustrated in Fig. 3 . The uranium sample is mounted close to an x-ray tube which is operated above the K_{abs} edge (115.6 eV) to produce fluorescent x-rays in the sample atoms. The sample is located at the focus of the two-meter focal length bent-crystal spectrometer of the Henrikson design[23] using the (310) planes of a $2\frac{1}{2}$ x 3" quartz crystal.

The theoretical prediction of the size of the shift for a non-deformed nucleus with a uniform charge distribution calculated in the previous section is 0.0023 x-units. To gain an idea of the size of this effect, one can calculate what rotation of the bent-crystal this wavelength difference corresponds to. The lattice spacing d of the (310) planes in quartz is 11738 Å . Differentiating Bragg's Law, one has for first order diffraction (N = 1),

$$\Delta\theta = \frac{N\,\Delta\lambda}{2d\cos\theta} \approx 0.2 \text{ seconds.} \qquad (17)$$

This is an exceedingly small rotation of the crystal. It will not be possible to observe the shift by mixing the two isotopes together in one sample and then resolving the two $K_{\alpha 1}$ lines because of the instrumental and natural line-widths. Operating the bent-crystal spectrometer under optimum resolution conditions by using a very narrow source and reduced bent-crystal aperture will still yield an instrumental line-width at least 40 times greater than the shift itself. It is seen

from Fig. 1 that the natural line-width is perhaps 50 times greater than the shift.

Therefore, the method we have chosen for detecting the shift involves measuring the energy of the $K_{\alpha 1}$ x-ray of each isotope separately and obtaining the value of the shift through taking the difference.

B. Sources of Error

Whenever the result of an experiment depends on a small difference between two measurements, sources of systematic errors become extremely important. The very small size of the isotope shift places requirements on the accuracy, stability, and reproducibility of the bent-crystal spectrometer which considerably exceed its original design limits; the performance of critical spectrometer parts must be checked and improved where found necessary. Before this experiment was begun, deviations in the reproducibility of spectrometer runs (using sources of comparable size and strength to the uranium sources used in this experiment) were considerably greater than the size of the isotope shift itself. Below are listed some of the important factors which were considered and met.

1. Temperature stability.
2. X-ray tube output stability.
3. Maintaining fixed sample position relative to the crystal.
4. Precision lead-screw linearity and freedom from local defects.
5. Non-stiction in the crystal-pivot bearing.

6. Wear in the lead-screw thrust bearing and end plate.
7. Reproducibility of the rotation of the lead-screw to the desired angles.
8. Accuracy of the division of the circle on the main dial.
9. Freedom from collimator effects.
10. Spectrometer alignment and vertical divergence.
11. Prevention of a non-uniform background.
12. Clock timing.

In investigating each of these problems, the goal was set that the experimental system be constructed, organized, or improved so that the net possible effect of any given source of error would be of the order of 1/10 the size of the shift or smaller (i.e., of the order of a 0.02" rotation of the crystal relative to the sample). The above items for investigation can be classified under four general headings and are discussed further in appendices.

1. Experimental Environment - Appendix I
2. Spectrometer Mechanism - Appendix II
3. Alignment of the Experiment - Appendix III
4. Systematic Error Considerations - Appendix V.

The measurement of rotations with a relative precision of nearly 0.01" is necessary for the checking of some of these listed items. This was accomplished through the use of a set of thermo-micrometers[24]. As an example of the value of the thorough checking of the performance of the spectrometer mechanism, Fig 4 is presented.

It illustrates the improvement in the linearity of the sine-screw mechanism which resulted when the wear problems of the sine-screw thrust bearing and end plate were solved.

C. The Final Experimental Set-Up

The experimental set-up that resulted from the investigations is illustrated in the line-drawing of Fig. 5 . Isolation of the crystal-pivot unit and the sample table from the rest of the apparatus and the building was found to be necessary. Therefore, the former were placed on a two-foot thick concrete slab. The temperature of the room was controlled to $\pm$ 0.1^{o}C. The radiation shielding discussed in Appendix III-B and illustrated in Fig. 6 was carefully positioned to prevent contributions to the background which might make it uneven. Automatic control and data recording equipment necessary for the method of fast and repeated sweeping over the peak, to be described in Chapter V, were also an important part of the experimental system.

V. EXPERIMENTAL PROCEDURE

A. Sample Preparation

Isotopically pure U-233 (99.46%) and U-238 (99.99%) samples were obtained from the Atomic Energy Commission, Oak Ridge. They were both in the form of an oxide powder U_3O_8. Six quartz capillary tubes, matched in pairs, were filled with this oxide powder, 3 with U-233 and 3 with U-238. Two of the capillaries were 7-mil I.D. and four were 10-mil I.D. Some difficulty was experienced in filling the 7-mil capillaries uniformly without clogging, particularly in the case of U-233. (Because of poor packing, the 7-mil U-233 sample was not used in the experiment.) Increasing the diameter to ten mils reduced this problem and four excellent ten-mil samples in which the material was uniformly distributed were obtained, two of each isotope filled to a height of one inch.

B. Sample Placement and Shielding

The sample capillary tubes were made longer than the 1 inch depth to which the oxide was filled so as to allow their support in a holder which would keep the sample material up free and in the clear. (See Fig. 7). The samples could then be placed and so shielded such that when viewed from the bent-crystal, only the upper portion of the capillary which contains the sample could be seen. As shown in Fig. 6 the lead housing around the sample has openings both front and back. Because the back-opening is larger, the only object within the lead housing which is visible to the bent-crystal is the 1 inch high sample

and quartz capillary. This is necessary so that the counting background will be smooth, balanced, and low. (See Appendices III-B and V-E for more discussion of the background.)

The x-ray tube is mounted overhead and about 45 degrees forward of the sample as illustrated in Fig. 5 . The x-ray tube can be cranked up to allow the changing of the sample and then lowered back into its former position. It does not come into contact with the sample, the lead housing of the sample (not shown in Fig. 5) or the sample table.

The base of the sample holder fits into a special well which allows easy switching of samples without placing much force on the table (and thereby moving it slightly) thus insuring that each sample is held in nearly the same position relative to the bent-crystal.

As is discussed in Appendix I-B the only objects on the concrete isolation slab are the sample table, necessary shielding, and the crystal-pivot unit.

C. Data-Taking Procedure

The results of a general scan in the region of the $K_{\alpha 1}$ x-ray are presented in Fig. 8 . The $K_{\alpha 1}$ x-ray is well isolated from the other x-rays present. So that good data on the background and the slope of the background will be collected during the experiment, the region over which the spectrometer will be made to sweep extends beyond the edges of the x-ray line as indicated in Fig. 8.

Another set of x-ray peaks exist for negative Bragg angles as illustrated in Fig. 9 . Both positive and negative sweeps are necessary for a wavelength determination because the effective zero of the instrument does not correspond to the zero reading of the main dial. The exact value of the effective zero (called the spectrometer beta-point) depends on the exact location of the sample.

Automatic spectrometer control and data recording equipment was developed for the execution of the experiment. Briefly, the spectrometer was programmed to sweep over the $K_{\alpha 1}$ line taking counts at 35 different points on the line. It advanced from point to point every 20 seconds and punched out the number of counts on computer cards by means of a modified IBM keypunch machine. The general pattern followed by the spectrometer was to perform four of these sweeps on the positive side in succession and then to go over to the negative side and perform four sweeps there.

This series of four positive sweeps, then four negative sweeps is repeated without interruption (the x-ray room is unentered and completely sealed) for approximately 24 hours. Then the sample is removed and replaced with the next one. The samples are rotated daily.

D. Data Reduction

The reduction of the data thus collected was analyzed in three steps which will be discussed briefly. For additional detail, reference is made to Appendix IV. First, an individual least-squares fit was performed by computer on the line resulting from each cycle. An

example of one of these lines is shown in Fig. 10. Typically from the counting statistics involved, the peak center of a given cycle is determined to ~ ± 0.001 x-units.

A plus and minus cycle paired together determine a value $\lambda_{\text{SINGLE MEASUREMENT}}$ for the wavelength of the $K_{\alpha 1}$ x-ray from one isotope. The second step in the reduction of the data involves solving for each of the $\lambda_{\text{SINGLE MEASUREMENT}}$ values which are contained in the consecutive plus-minus pairs in the string of cycles which constitute the run. In effect, a run simply consists of a string of repeated measurements, $\lambda_{\text{SINGLE MEASUREMENT}}$. This provides a check on the reproducibility of the instrument within a given run and allows the determination of a standard deviation which includes the effects of instrument irreproducibility and shifts from vibration, etc.

In the third step, the value of the isotope shift can be taken to be the difference in the averages for the U-238 and the U-233 samples, respectively. However, one can do a little better by deriving a weighting factor for each $\lambda_{\text{SINGLE MEASUREMENT}}$ where this weighting factor represents the dependability of that particular measurement. The weighted mean values for the U-233 and U-238 measurements are then found. The shift is the difference between these two weighted mean values. The weighting factor can be obtained from the standard deviation which results from the reduction of the individual runs. This weighting factor is discussed more fully in Appendix IV-C.

VI. RESULTS

Measurements were taken using four 10-mil samples and one 7-mil sample. The set of 4 closely-matched 10-mil samples, two of each isotope, allowed the measurement of the effect under conditions in which all sample parameters were maintained as nearly identical as possible for the two isotopes while also providing the check of being able to compare the results for two different samples of the same isotope. As a test of the sensitivity of the wavelength result to these sample parameters, two additional runs were made where sample parameters were radically different. In the first, the sample diameter was decreased by 30% (by using the 7-mil U-238 sample) producing a significantly different peak height and width. In the second sample effect test run, measurements were conducted with a 10-mil U-238 sample lowered from its normal height by 5/16".

The results of these various runs, presented in detail in Appendix VI and summarized in Table III, show good agreement between all runs conducted with the same isotope and show a consistent shift when runs with different isotopes are compared. No sample effects appear in the special test runs. This indicates that the final result is free of possible bias due to sample effects. Additional consideration to these effects is given in Appendix V.

It should be noted that the values $\lambda \pm \sigma$ listed in Table III are not intended to represent the <u>absolute</u> value of the wavelength of the $K_{\alpha 1}$ x-ray. As discussed in Appendix II-D, the action of the spectrometer correction-cam was intentionally defeated. This may

Table III

Summary of Results for the Five Samples

Sample	$\lambda \pm \sigma$ a) x-units	Runs	Cycles	Total Counts
First 10-mil U-238 Sample	125.68044 ± 0.00058	1	23	1×10^7
Second 10-mil U-238 Sample	125.68067 ± 0.00017	5	101	5×10^7
Second 10-mil U-238 Sample lowered by 5/16"	125.68034 ± 0.00031	1	29	1×10^7
7-mil U-238 Sample	125.68049 ± 0.00069	1	23	5×10^6
First 10-mil U-233 Sample	125.67799 ± 0.00028	5	117	3×10^7
Second 10-mil U-233 Sample	125.67850 ± 0.00020	6	128	3×10^7
All U-238 Runs Combined	125.68060 ± 0.00014	8 runs	175 cycles	8×10^7 cts
All U-233 Runs Combined	125.67832 ± 0.00017	11 runs	245 cycles	6×10^7 cts

a) λ is the weighted mean of all $\lambda_{\text{SINGLE MEASUREMENT}}$ values for that sample and σ is its standard deviation as defined in Eqns. (50)-(52). The absolute value of λ may contain a systematic error not included in σ as explained in the text.

introduce a systematic error into the absolute value of the measured wavelength. However, it will be identical for each sample. Therefore, this systematic error will cancel in the isotopic shift determination.

The final result for the isotopic shift taken as the difference between the weighted mean of all the $\lambda_{\text{SINGLE MEASUREMENT}}$ values for each isotope is presented in Table IV.

Table IV

Final Result for Isotope Shift

$\lambda_{K_{\alpha 1}}$ (U-238) - $\lambda_{K_{\alpha 1}}$ (U-233) = 0.00228 ± 0.00022 x-units
$E_{K_{\alpha 1}}$ (U-238) - $E_{K_{\alpha 1}}$ (U-233) = - 1.8 + 0.2 eV

VII. DISCUSSION OF THE RESULT

The experimental result in Table IV and the theoretical prediction of Chapter III seem to be in excellent agreement. However, the theoretical prediction is based on the simple model of a uniformly charged non-deformed nucleus of radius $R = R_0 A^{1/3}$. Thus, this model has ignored even-odd staggering effects, deformation, polarizability, and compressibility of the nucleus. The comparison of the experimental result to theory must also include a consideration of the effects mentioned above. The first two effects can be determined by means of studying optical data which is available for uranium.

A. Even-Odd Staggering

The even-odd staggering effect is exhibited in a number of optical experiments[25] where the isotope shift has been observed for a series of isotopes (A, A + 1, A + 2, ...) of the same element. With the excellent resolution available in optical work a line characteristic for a transition between two electronic states can be resolved into a set of lines, each corresponding to a different isotope. These lines do not lie separated by equal amounts, but appear to be staggered. The line from the odd-isotope lies closer to the line of the lighter even-isotope neighbor than to the line of the heavier neighbor.

Optical shift measurements for uranium exhibit this even-odd staggering effect. Figure 11a illustrates the data by D.D. Smith et al.[26]. This same line has been measured independently by A.R. Striganov et al.[27] and the results are in agreement to 2.5% or better.

Although the cause of this even-odd staggering is not understood, it is probably a nuclear effect[28]. The even-odd staggering has been observed for many even-Z nuclei, but until it was observed for the first time in an odd-N, odd-Z nucleus by Hull and Stroke[29], there was confusion as to whether it was the odd-N or odd-A isotope which was staggered in the direction of its lighter neighbor[30]. The shift data for 7 Tl isotopes (Z = 81) by Hull and Stroke, are compared with data for 6 Hg isotopes (Z = 80) by Kopfermann[31] in Fig. 11b. This comparison strongly suggests that the staggering effect is dependent on the neutron number and it appears to be relatively independent of whether the nucleus has an odd or even number of protons.

It would be an interesting theoretical problem to investigate whether the pairing model of the nucleus is able to explain the even-odd staggering effect. The addition of an odd neutron to a nucleus obeying the pairing model might not greatly affect the size of the core since the odd neutron prefers to remain outside the core. The addition of the odd neutron would therefore not appreciably increase the size of the charge distribution of the core. Thus, only a small isotope shift would result. However, with the addition of the second neutron, the neutron pair so formed interacts with the core expanding its average radius. This enlarges the proton distribution which in turn causes a large isotope shift. It would seem that the results would be independent of whether Z is even or odd. To date, no theoretical calculations have been performed on the pairing model to test this possible cause of the even-odd staggering anomaly.

B. Deformation

Wilets, Hill and Ford[32] have studied the effect of the deformation of the nucleus on the isotope shift. For an s electron, the charge density of a deformed nucleus is equivalent to the charge density obtained by averaging over all angles. Therefore, a deformation has the effect of increasing the value of $\langle r^2 \rangle$ and contributing to the shift. Wilets, Hill, and Ford assumed a cylindrically symmetric ellipsoidal deformation in which the nuclear radius R is:

$$R(\theta) = R_0 \left[1 + \alpha P_2(\cos \theta) \right] . \tag{18}$$

Assuming a constant volume and a uniform charge density, Wilets, Hill and Ford show that the ratio of the isotope shift due to a deformation change to the isotope shift due to the normal volume effect is:

$$\frac{(\Delta E)_{DEF}}{(\Delta E)_{VOL}} = \frac{3}{10} (2\rho + 3) A \left(\frac{\Delta(\alpha^2)}{\Delta N} \right)_z \tag{19}$$

where $\rho = (1 - \alpha^2 z^2)^{1/2}$ and A is the atomic weight. The shift, it should be noted, is sensitive to the change in deformation.

We now express this same result in terms of the deformation parameter β as used by Bohr and Mottelson[33]. In terms of β the nuclear radius is

$$R = R_0(1 + \beta Y_2^0) . \tag{20}$$

A comparison of the spherical harmonic Y_2^0 and the Legendre polynomial P_2 gives the relation:

$$\alpha = \sqrt{\frac{5}{4\pi}}\ \beta \tag{21}$$

and hence

$$\frac{(\Delta E)_{DEF}}{(\Delta E)_{VOL}} = \frac{3}{8\pi}\ (2\rho + 3)\ A \left(\frac{\Delta(\beta^2)}{\Delta N}\right)_Z . \tag{22}$$

Inserting $\rho = 0.74$ and $A = 235$, we have for uranium

$$\frac{(\Delta E)_{DEF}}{(\Delta E)_{VOL}} = 125\ \frac{\Delta(\beta^2)}{\Delta N} . \tag{23}$$

The relationship between the intrinsic quadrupole moment Q_0 and the deformation parameter β is[33]:

$$Q_0 = \frac{3}{\sqrt{5\pi}}\ Z\ R^2\ \beta(1 + 0.16\beta + \ldots) . \tag{24}$$

Column 2 of Table V lists the experimental values for Q_0 for uranium. Using these values for Q_0 and Eqs. (5) and (24), the values for β for seven isotopes of uranium were obtained and are listed in column 4 of Table V. Also given are the $\Delta E_{DEF}/\Delta E_{VOL}$ ratios determined from the deformation values β and Eq. (23). For comparison, the experimental optical isotope shift values by D.D. Smith et al.[26] are included in Table V. It can be seen that the deformation effects on the isotope shift are sizeable.

Another comparison illustrated by means of Fig. 12, will show this more clearly. The center set of lines represents the evenly spaced isotope shift spectrum which results if the nuclei obey the $R = R_0\ A^{1/3}$ relation. At the bottom of Fig. 12 (in the same scale but adjusted so the U-238 lines are lined up) is presented the spectrum as it should appear if the effects of the deformations listed in Table V are

Table V

ISOTOPE	Q_0 barns	β [c]	$\frac{\Delta E_{DEF}}{\Delta E_{VOL}}$ [d]	Optical Shift Data [e]
U-238	10.52 ± 0.48 a)	0.274	-	-
U-236	10.35 ± 0.44 a)	0.271	+ 0.11	0.147 ± 0.010
U-235	10.5 ± 1.2 b)	0.276	- 0.05	0.251 ± 0.002
U-234	9.77 ± 0.38 a)	0.257	+ 0.28	0.300 ± 0.003
U-233	11.9 ± 1.0 b)	0.314	- 0.59	0.396 ± 0.005
U-232	9.98 ± 0.28 a)	0.264	+ 0.11	-
U-230	9.46 ± 0.52 a)	0.252	+ 0.18	-

a) By method of lifetime measurement of first excited state. Ref. 34.

b) By method of Coulomb excitation. Ref. 35 and 36.

c) Deformation parameter calculated using Eq. (24). $R = 1.2\ A^{1/3} f$.

d) Calculated using Eq. (23). Shift is between indicated isotope and U-238.

e) Optical isotope shift data of line 4244.372 Å expressed relative to U-238 in Å units. Ref. 26.

included. It is seen that the isotope shift spectrum is extremely sensitive to the changes in the deformations. The experimental isotope shift data of D.D. Smith et al.[26] is displayed again for convenience at the top of Fig. 12 with the scale arbitrarily adjusted to make the lines for U-238 and U-236 line up. This optical isotope shift data is strong evidence that the quadrupole moments of the uranium series of isotopes change very smoothly from one isotope to the next. The intrinsic quadrupole moments data of Table V are presented in Fig. 13, and a solid line is drawn through the data to indicate how the quadrupole moments may actually vary with A for uranium in order to account for the optical isotope shift data. Since accurate theoretical estimates of the size of the optical isotope shift are not available, the slope of this line cannot be uniquely determined from the optical isotope shift data nor does the isotope shift data indicate the height of the line. What the optical data does indicate is that the line should be straight. The line drawn is the one which seems to best fit the quadrupole data. Lines of other slopes and heights are not excluded by the optical isotope shift data.

If one were to attempt to explain the even-odd staggering observed in uranium by ascribing different quadrupole moments to the odd-N isotopes of uranium, the quadrupole moments of the odd-N isotopes would be lowered as indicated by the dashed lines in Fig. 13.

On the basis of the optical isotope shift data for uranium, it appears that the quadrupole moment reported for U-233 by Newton[36] is too high. In a Coulomb excitation experiment, the intrinsic quadrupole

moments $Q_0(2)$ and $Q_0(1)$ of the second and first rotational states were estimated to be 11.9 ± 0.4 and 15.7 ± 1.6 barns, respectively. Newton was unable to account for this sizeable discrepancy, but since $Q_0(2)$ involved fewer assumptions than $Q_0(1)$, Newton took $Q_0(2)$ as the more reliable result. It is also the one we have taken for Table V and Fig. 13. But the optical isotope shift data appear to require that the Q_0 be even lower than Newton's value for $Q_0(2)$.

Therefore, we shall not use the Coulomb excitation value for the intrinsic quadrupole moment of U-233. Instead, we shall assume that the deformation of the uranium isotopes varies as indicated by the solid line in Fig. 13. In addition, we shall also assume that the even-odd staggering and deformation differences affect x-ray and optical isotope shifts in the same way. With these assumptions, we can use the optical shift data of Table V to predict what the combined effect of even-odd staggering and deformation differences are on the x-ray isotope shift between U-233 and U-238. Taking the intrinsic quadrupole moments of U-238 and U-233 to be 10.5 and 10.0 barns, respectively, we find that by means of Eqs. (5), (24), and (23) that $(\Delta E)_{DEF}/(\Delta E)_{VOL.} = +0.15$. If we take the optical data of Table V and multiply the U-238 to U-234 shift by 5/4 to see what value a non-staggered U-238-U-233 shift would have, we obtain 0.374 Å. Thus, the optical result of 0.396 Å for U-238-U-233 represents a factor of 0.396/0.374 = 1.06 enhancement of the shift due to even-odd staggering. Combining the 15 percent increase due to a deformation change with the 6 percent increase from the even-odd staggering, we conclude that the isotope shift calculation of Chapter III

for a non-deformed nucleus should be increased by 21 percent giving a correction factor C_{SD} of:

$$C_{SD} = 1 + \frac{(\triangle E)_{STAGGER + DEF}}{(\triangle E)_{VOL}} = 1.21 \ . \qquad (25)$$

c. Compressibility

If E_{NC} is the energy and R_{NC} is the radius of the nucleus in the absence of Coulomb forces, then in the presence of Coulomb forces, the energy of the nucleus as a function of its radius is given by[37]:

$$E = E_{NC} + E_C \left(\frac{R_{NC}}{R}\right) + \frac{1}{2} E''_{NC} \left(\frac{R - R_{NC}}{R_{NC}}\right)^2 + \ldots \qquad (26)$$

where $E''_{NC} = \left[R^2 \, \partial^2 E_{NC}/\partial R^2\right]_{R_{NC}}$ and E_C is the Coulomb energy:

$$E_C = \frac{3}{5} \frac{Z^2 e^2}{R_{NC}} \ . \qquad (27)$$

Assuming $(R - R_{NC})$ to be small, the equilibrium radius is approximately:

$$R = R_{NC}\left(1 + \frac{E_C}{E''_{NC}}\right) \ . \qquad (28)$$

From the property of nuclear saturation, it is customary to introduce the compressibility factor K as

$$E''_{NC} = K A \ . \qquad (29)$$

From Eqs. (27) - (29) and taking $R_{NC} = R_0 A^{1/3}$, we can derive for the change in radius of a compressible nucleus due to a change in neutron number[38]:

$$\frac{\partial R}{\partial N} = \frac{R}{3A}\left[1 - \frac{4\,E_C}{E''_{NC} + E_C}\right] \quad . \tag{30}$$

This is to be compared with the relation:

$$\frac{\partial R}{\partial A} = \frac{R}{3A} \tag{31}$$

which results from differentiating $R = R_0 A^{1/3}$. In the derivation of Eq. (8) in Chapter III, the incompressible result of Eq. (31) has been substituted for the factor $\Delta R/\Delta A$ in Eq. (6) instead of the compressible result (Eq. 30). Therefore, to account for compressibility, a correction factor, C_{COM}, equal to

$$C_{COM} = \left[1 - \frac{4\,E_C}{E''_{NC} + E_C}\right] \tag{32}$$

must be applied to the incompressible result of Table II.

A theoretical calculation of the compressibility factor K by Falk and Wilets[39] gives a value of K = 214 MeV while that of Brueckner and Gammel gives K = 172 MeV. Semi-empirical results of 175, 218, and 302 MeV have also been obtained[39]. Using Eqs. (5), (27), (29), and (32), we obtain the compressibility corrections listed in the table below for various values of K.

Table VI

Correction factor C_{COM} to account
for the compressibility of the nucleus

K in MeV	C_{COM}
50	0.69
100	0.84
150	0.89
200	0.92
300	0.95

We have listed the lower values of K (50 and 100 MeV) because of the interesting and not understood discrepancy which exists between the experimental and theoretical optical isotope shift results. It is found that on the average

$$\frac{(\Delta E)_{EXP}}{(\Delta E)_{THEORY}} = \sim 0.7 \qquad (33)$$

where the theory is based on an incompressible model[40]. It has been the practice in optical isotope shift work to ascribe all of this discrepancy to the compressibility of the nucleus. This requires a compressibility factor K which is much lower ($K \approx 50$-75 MeV) than the theoretical or semi-empirical results. It will be interesting to see if the x-ray isotope shift result also requires this value for the compressibility factor.

D. Polarizability

It was suggested by Breit et al.[41] that polarization of the nucleus by the electron might influence isotope shifts. This possibility has been investigated by Reiner and Wilets[111] who found that the size of the polarizability contribution in terms of the deformation contribution to the shift is:

$$\frac{(\Delta E)_{POL}}{(\Delta E)_{DEF}} = -\frac{z\alpha}{4\pi} = -0.05 \text{ (for } z = 92). \tag{34}$$

Since we found $(\Delta E)_{DEF}/(\Delta E)_{POL} = 0.15$, we can safely neglect the effects of polarizability of the nucleus by the electron.

E. Electron Scattering Results and the Radius of the $_{92}U$ Nucleus

In Eq. (8) the square of the wavefunction was evaluated at the nuclear radius $[F_0^2(R) + G_0^2(R)]$, to give the first order perturbation result of Chapter III. The value used for the nuclear radius was 7.38×10^{-13} cm obtained from the $R=1.2 \times 10^{-13} A^{1/3}$ cm relation. However Elton[42] has found from electron scattering results that the expression

$$R = 1.115\ A^{1/3} + 2.151\ A^{-1/3} - 1.742\ A^{-1} \tag{35}$$

gives a better fit to the data. This slightly decreases the radius to the value $R = 7.20 \times 10^{-13}$ cm for uranium. This leads to the small correction C_{ES}:

$$C_{ES} = \frac{[F_0^2(R) + G_0^2(R)]_{R = 7.20f}}{[F_0^2(R) + G_0^2(R)]_{R - 7.38f}} = 0.96\ . \tag{36}$$

F. Comparison of Theory with Experiment

Combining the corrections for even-odd staggering and deformation (C_{SD}), for compressibility (C_{COM}), and for the radius modification from electron scattering data (C_{ES}), we arrive at the values for the shift displayed in Table VII in which different values of C_{COM} have been used corresponding to different compressibility factors K.

Table VII

Predictions Assuming Different Compressibility Factors

K in MeV	$(\Delta E)_{THEORY}$ in eV
50	1.44
100	1.75
150	1.85
200	1.92
300	1.98

Comparing this with our experimental result of 1.8 ± 0.2 eV, it is tempting to conclude that the lower value for the compressibility is excluded. However, such a conclusion cannot be fully justified on the basis of this one experiment because of the uncertain validity of the two assumptions which were used to obtain C_{SD}.

To test the assumption that the even-odd staggering behaves in the same way for both x-ray and optical isotope shifts will require the measurement of the x-ray isotope shift for additional isotopes.

A measurement of U-234 - U-238 would be helpful. To test the other assumption made in determining C_{SD} would require more accurate deformation data. If the correct value for the compressibility factor C_{COM} could be obtained either through improved theory or from the systematics of a large number of x-ray isotope shift measurements, then it is possible that the isotope shift measurements will give the best values for the changes of the quadrupole moments from one isotope to the next.

The result of this experiment does show that the large intrinsic quadrupole moment listed in Table V for U-233 is too high relative to Q_0 for U-238. This value for the quadrupole moment implies a deformation contribution of $(\Delta E)_{DEF}/(\Delta E)_{VOL.} = -0.59$ as listed in column 4 in Table V. Using this value instead of the deformation contribution value of + 0.15 which was determined in Section A of this present Chapter, the size of the predicted shift (for K = 200 MeV) would be 0.7 eV. This is in clear disagreement with our result of 1.8 ± 0.2 eV.

VIII. CONCLUSION

The goal of this thesis project was to succeed in the first experimental detection of the isotope shift of an electronic x-ray. This has been accomplished through the use of the Caltech two-meter focal length bent-crystal spectrometer for the isotope pair of U-238 - U-233. The $K_{\alpha 1}$ x-ray from the U-238 sample is 1.8 ± 0.2 eV lower in energy than the $K_{\alpha 1}$ x-ray from U-233. This is in good agreement with the theoretical prediction if certain assumptions are made about 1) the not yet understood even-odd staggering, 2) the values for the intrinsic quadrupole moments, and 3) the values for the compressibility factor K.

The first assumption is that the ratio of the magnitude of the even-odd staggering effect to the magnitude of the normal volume-dependent effect is the same for both x-ray and optical isotope shifts. This assumption seems to be reasonable because the staggering effect is believed to be of nuclear origin.

The second assumption involved taking the quadrupole moments of the uranium isotopes to be those indicated by the solid line in Fig. 13. Justification for making the line in Fig. 13 smooth comes from optical isotope shift data. The slope of the line is less certain, but the present x-ray isotope shift result indicates that the Coulomb excitation value for Q_0 of the U-233 nucleus is much too high. Thus the present result lends support to the assumed slope of the line in Fig. 13.

Improved knowledge of nuclear compressibility effects could be gained from the systematics of many x-ray isotope shift measurements on a large number of isotopes.

We therefore conclude this thesis by considering whether the Caltech bent-crystal spectrometer can be used for detecting further isotope shifts in other regions of the periodical chart. F.A. Babushkin has recently made predictions for the size of the shift in the region $37 \leqslant Z \leqslant 82$ for $\Delta A = 2$. We present his results[43] in Fig. 14. The solid curve represents the shift calculated for an incompressible, spherical nucleus which exhibits only the volume-dependent isotope shift. The dots represent the predicted shifts if experimental values for the deformations of the nuclei are assumed*. The shift is for $\Delta A = 2$, so predicted shifts between isotope pairs of different spreads in ΔA must be adjusted accordingly. The horizontal line indicates the error bars achieved in this present work.

It can be concluded that many more cases can be measured, particularly for isotope pairs with ΔA greater than two. Of particular interest will be the $N \approx 90$ region where the nucleus undergoes a large change in deformation which greatly enhances the size of the effect. The result of this present experiment demonstrates that it

---

* In his deformed calculations, Babushkin included the 0.7 compressibility factor as commonly used in optical isotope shift calculations. Because the validity of this 0.7 factor is not confirmed in the case of x-rays, we have deleted this factor from his results, i.e., the deformed nucleus calculations presented in Fig. 14 also assume an incompressible nucleus.

will be possible to measure x-ray isotope shifts in many elements with the bent-crystal spectrometer and that such measurements will add to our knowledge of the nucleus.

APPENDIX I.

EXPERIMENTAL ENVIRONMENT FOR THE SPECTROMETER

A. Temperature Environment

A calculation of the effects of the thermal expansion of the spectrometer lead screw, lever arm, and the quartz crystal lattice spacing shows that there can be spurious shifts due to room temperature changes. To first order, the change of wavelength $\Delta\lambda$ for a temperature change Δt is:

$$\Delta\lambda = \lambda(C_{arm} - C_{screw} - C_{crystal})\Delta t. \qquad (37)$$

The spectrometer lever arm is aluminium ($C_{arm} = 25 \times 10^{-6}/^{o}C$), the lead screw is steel ($C_{screw} = 10 \times 10^{-6}/^{o}C$), and the crystal is quartz ($C_{crystal} - 10 \times 10^{-6}/^{o}C$). Therefore, in the region of interest for this experiment ($\lambda = 125$ x-units),

$$\Delta\lambda = 0.0006 \text{ x-units}/1^{o}C, \qquad (38)$$

which means a variation of only $4^{o}C$ would produce a shift equal to the isotope shift. Furthermore, this value depends on appreciable cancellation of the thermal expansion coefficients. Therefore, the result cannot be expected to be very reliable.

Thermal effects can affect the measured wavelength by other means as well. A horizontal movement of only 2 microns of the sample in a direction perpendicular to a line drawn from the sample to the bent crystal, shifts the beta-point (defined in Fig. 9) by an amount greater than the shift. Thermal expansion of the members of the

sample table or crystal-pivot frame, or even expansion of the floor itself could shift the beta-point. Of itself, a shift in the beta-point does not affect the measured wavelength since it displaces both the positive scan and negative scan in the same direction, but a beta-point changing periodically with an unfavorable frequency could produce a systematic error.

The solution of the problem of temperature effects lies in carefully maintaining the temperature within small limits. Achievement of this solution was facilitated by the location of the spectrometer in a corner room of the sub-basement of the building. All air communication to the spectrometer room was sealed off. The adjoining spectrometer control room was also sealed and its air temperature regulated by air conditioning to $\pm 1^{\circ}C$. To insure equilibrium, the temperature of the room had been held to the value it had during the actual data-taking ($26.1^{\circ}C$) for several weeks prior to the beginning of the experiment. During a run, it was not necessary to enter the spectrometer room. Its temperature was observed by telescope to be very stable and it remained within limits of $\pm 0.1^{\circ}C$.

B. Requirements for Rigidity of the Floor

The experiment was originally set up using the existing floor as a base. This however, was shown to be inadequate for the present experiment because of excessive bending and flexing of the floor itself, producing shifts in the position of the sample relative to the crystal-pivot frame. This problem was discovered through the use of a Davidson model D600 auto-collimator. It was placed on the sample

table and used to observe images reflected by a set of plane mirrors placed on the crystal pivot in place of the bent crystal. It was discovered that even the disturbance of a person's weight in the vicinity of the spectrometer distorted the floor enough to produce a shift in the orientation of the bent-crystal by an amount which was an order of magnitude greater than the expected isotope shift! During the experiment, the situation would be considerably worse. Although the room is not entered during the data taking, the heavy collimator-detector (~ 600 pounds) will swing from one side to the other as plus and minus scans are taken.

The solution involved removing a 9 foot by 4 foot rectangular portion of the floor, digging down to solid dirt below and casting a heavily reinforced concrete slab in its place about two feet thick and decoupled from the floor of the building by a 3/4" layer of felt. Only sensitive or necessary objects were placed on the slab. The sensitive objects are the sample table and the crystal-pivot unit and the necessary objects are the various lead shielding plates. The x-ray stand and collimator-detector unit were placed off the slab as shown in Fig. 5.

With the installation of the concrete slab, shifts could no longer be detected with the D600 auto-collimator. Further tests using a special thermo-micrometer[24] which had much greater sensitivity (~ 0.0001 x-units) showed that the swinging of the collimator-detector from side to side produced shifts of 0.00015 x-units magnitude. Since these shifts were consistently the same magnitude each time, the

effects from the collimator-detector swinging are safely negligible.

However, the thermo-micrometer did show that even with the isolation provided by the concrete slab, large shifts (sometimes equivalent to many times the size of the isotope shift) occurred occasionally due to objects being dropped in or around the building, doors being slammed, etc., and perhaps due to local seismic activity. However, the infrequent occurrence of these disturbances did not merit the expense of a further isolation of the experiment from the outside world. The experimental procedure and method of data reduction described in Appendix IV was adequately able to average out the effects of these disturbances.

APPENDIX II.

TESTING THE SPECTROMETER MECHANISM

A. Basic Features of the Spectrometer Mechanism

The California Institute of Technology two-meter focal length bent-crystal spectrometer of the Henrikson design was used. Since the operation and design of this spectrometer have been presented in detail elsewhere[23], only basic features of its operation which are relevent to the present experiment are to be discussed here.

The heart of the instrument is the precision sine-screw mechanism which converts precise rotations of the lead-screw into a motion of the lever arm which rotates the bent-crystal around an axis defined by the pivot bearing. (See Fig. 5 .) The sine of the Bragg angle is determined through the sine-screw mechanism. The dial reading on the lead screw is directly proportional to the wavelength of the radiation which satisfies Bragg's Law and is diffracted by the bent-crystal into the collimator-detector. The instrument was designed so that a one-half revolution of the lead-screw corresponds to a change of one *x*-unit when the diffraction is from the (310) planes of a quartz crystal. Consideration must be given to:

1. the main dial accuracy,
2. the stepping motor accuracy and reproducibility,
3. the precision lead-screw linearity,
4. the thrust bearing and end plate precision and wear problems, and
5. the possibility of striction in the crystal pivot bearing which could produce distortions in the frame of the entire unit.

These problems will now be discussed.

B. The Main Dial Precision

It is desirable to be able to read the main dial which is attached directly to the lead-screw to a resolution of 0.0002 x-units for purposes of:

1. being able to check the accuracy and reproducibility of the stepping motor which drives the lead screw, and
2. being able to accurately read-out the values of the settings used during the experiment.

This is equivalent to dividing the circle accurately to 1 part in 10,000 or to about two minutes. A dial was ruled to within this tolerance by a precision dividing head (whose absolute precision is ± 6") available at the Jet Propulsion Laboratory. With the use of a microscope, the new spectrometer main dial could be read to a precision of 1 part in 20,000. This precision dial could then be used to check the accuracy of the division of the circle and the reproducibility of the 200-position stepping motor which would drive the spectrometer.

C. The Stepping Motor

The reproducibility of the spectrometer is only as good as the reproducibility of the stepping motor used to drive the lead-screw. The characteristics of a commercially available[44] inductor motor were examined using the precision main dial. The motor can be operated as a phase-switched stepping motor with 200 switching operations corresponding to one revolution. It is designed with bifilar windings to allow the use of a single-ended power supply as the driver. Therefore,

equivalent current configurations in the motor's windings occur every fourth step. By operating the motor so that the spectrometer counting positions always correspond to the stepping motor being in the same current configuration, it is possible to achieve both a precision in the reproducibility and an accuracy in the division of the circle good to ± one part in 20,000. This is equivalent to ± 0.0001 x-units.

D. The Lead-Screw, Thrust Bearing and Crystal-Pivot

As soon as it has been ascertained by means of the main dial that the stepping motor is reproducibly and accurately rotating the lead-screw, then the performance of the combination of the lead-screw, thrust bearing, and crystal-pivot bearing can be checked. This is done by directly measuring the rotation of the bent-crystal turntable resulting from successive steps of the stepping motor. For the requirements of the present experiment, this rotation must be measured to a relative accuracy of 0.02 seconds. A set of four thermo-micrometers[24] was used to obtain this sensitivity and relative accuracy.

The magnitudes of ~ 150 successive rotations of the bent crystal turntable were measured semi-automatically to provide data for a calibration run. Many calibration runs were taken. The results of each run were reduced by computer to provide a calibration plot of the actual turntable positions versus spectrometer main dial readings.

Deviations from linearity* in these calibration plots indicate defects somewhere in the mechanism.

Initial calibration runs produced very poor results in terms of what is required for this present experiment. An example was given in Fig. 4 . The initial calibration curves were very rough and periodic with each revolution of the lead screw. Small local imperfections repeated with every revolution. Repeated calibration runs over various portions of the lead-screw lead to the conclusion that the principle defect was the wearing of the lead-screw thrust bearing and end plate. Additional tests on the wearing properties of various materials resulted in the choice of using a polished end plate made of Morganite. It is a commercially available material of high compressive strength (up to 45,000 psi) made by compacting a graphite-carbon composite under high temperature and pressure. Careful polishing of the thrust-bearing while mounted on the lead-screw was also important. Following these improvements, the calibration curve did not show any deterioration or change in characteristics even after extensive use.

The spectrometer has a special correction cam illustrated in Fig. 15, which is used to correct for accumulated errors in the lead-screw[23]. It works very well for applying small corrections to the lead-screw so that the spectrometer is well calibrated throughout its entire region. However, this experiment does not require calibration

---

* Technically, the calibration curve is not linear, but follows the sin θ dependence required by Bragg's Law. However, the region of scan involves such a small change in θ that this deviation from linearity is not detectable.

throughout the entire spectrometer range; it only requires that the rotation be linear and accurate over very small regions, i.e., just over the $K_{\alpha 1}$ x-ray line on the plus and minus side. The action of the correction cam was defeated for this experiment to prevent the possibility of its introducing systematic errors. This means, however, that the absolute wavelength measurements of the $K_{\alpha 1}$ x-ray for U-233 and U-238 can both have a systematic error of as much as 0.01 x-units[45]. This will not affect the result of this experiment since the same systematic error is present for both isotopes and it is the relative shift between them which is the desired quantity.

The resulting calibration curve (Fig. 4), after these corrections were applied to the spectrometer mechanism is much improved. It still exhibits evidence of some wow in the screw which cannot be easily corrected, but the magnitude of the wow is quite acceptable as is demonstrated in Appendix V-A where the measured wavelength is examined as a function of the spectrometer beta-point. The crystal-pivot bearing shows no hint of stiction in Fig. 4.

A number of reproducibility runs in which the spectrometer was put through motions similar to those occurring during the actual data taking runs was performed. The crystal-turntable positions were measured with the thermo - micrometer. These runs indicated that the crystal rotation was reproducible to 0.0001 x-units or better over short time spans. Its reproducibility over long time intervals could not be checked because 1) of the presence of disturbances such as building vibration, and 2) because the stability of the thermo-micrometer over long periods of time is not known.

APPENDIX III

ALIGNMENT OF THE EXPERIMENTAL SYSTEM

As has been shown in Fig. 5 , the experimental system consists of four independent units; the x-ray stand, the sample table, the crystal-pivot unit, and the collimator-detector rack. To this list could also be added several moveable lead plates which are placed for shielding purposes. This appendix will discuss certain aspects of the placement of these units which are critical for the present experiment.

A. Collimator

The collimator does not play a role in the resolution of the spectrometer. The spectrometer derives all of its resolution from the bent-crystal. The collimator serves instead to reduce background from straight-through radiation when high-energy lines requiring small Bragg angles are being scanned. The Caltech spectrometer has been provided with a collimator which has a transmission curve width of $\sim$ 5 x-units. This allows the measurement of gamma radiation to energies well over 1 MeV. Because of the many shielding strips necessary to accomplish this, its transmission efficiency is only 50 percent and the flat portion of its transmission curve is only 0.5 x-units wide. For the usual measurement, this is perfectly acceptable. But the danger of the collimator tailoring to a small extent the edges of the x-ray peaks of this present experiment (FWHM of x-ray line is 0.37 x-units) is too great. The resolution of the collimator was greatly reduced (the total width of its new transmission curve is $\sim$ 100 x-units) by the removal of all but three of its shielding strips. This helps the counting

rate as well because its new transmission efficiency is nearly 100%. Even so, the flat portion of its new transmission curve is measured to be only 5 x-units wide. Therefore, careful alignment for concentricity of the collimator-detector rack with the bent-crystal turntable axis is necessary.

B. Shielding for a Low and Uniform Background

Because shifts of the order of 1/150-th of the width of the x-ray line are to be measured with an error of only 1/1500-th of the width, the background must be very clean and uniform. Direct radiation from the x-ray tube is confined to the inside of a special lead housing box which contains the uranium sample. This shielding box has two windows, one facing the bent-crystal which must receive the fluorescent x-ray radiation from the sample, and a second window which is located on the opposite wall of the box. This second window is larger so that when the box is viewed from the bent-crystal, the back wall is not visible. From the bent-crystal, the only object within the shielded box that is visible is the sample itself which is supported up free and clear in the air by means of the holder shown in Fig. 7 . A lead backstop located 3 feet behind the lead housing and upon which no direct x-ray radiation from the x-ray tube can fall serves as the background to the sample.

Because direct radiation from the x-ray tube can fall on the edges of the front window, additional shields located in front of the lead box define an even smaller window. One last large shield with a small window is located halfway between the sample and the crystal.

It serves to prevent problems of scattered radiation entering the detector from those regions in the room toward which the collimator is aimed. Fig. 6 illustrates some of the features of these various shields.

C. Alignment to Reduce the Vertical Divergence

Vertical divergence considerations make three different alignments important. First, the height of the sample table must be properly adjusted relative to the bent-crystal. Second, the axis of rotation of the bent-crystal turntable must be vertical. Third, vertical window defining slits should be used in front of the sample so that the apparent length and height of the samples as seen by the crystal are the same. These three alignments will be discussed after a derivation of the vertical divergence effect.

For the moment, consider the sample to be a point instead of a line. Then, proper alignment would dictate that the sample table height be adjusted such that a plane normal to the rotation axis of the crystal-pivot turntable and passed through the center of the crystal will also pass through the point sample. Should the sample be too high or too low by a distance d, then radiation from it will strike the crystal obliquely with an angle of vertical divergence φ defined by:

$$\varphi = \arctan\left(\frac{d}{\ell}\right) \qquad (39)$$

where ℓ is the sample to crystal distance. If the central ray incident on the crystal makes a Bragg angle θ with the reflecting atomic planes, then the oblique ray from the displaced sample of vertical divergence angle φ makes a Bragg angle θ'. By spherical trigonometry, the

following relation is obtained[46]:

$$\sin\theta' = \sin\theta \cos\Phi \,. \tag{40}$$

The wavelength shift (by application of Bragg's Law) due to vertical divergence φ is:

$$\delta = \frac{\lambda - \lambda'}{\lambda} = \frac{\sin\theta - \sin\theta'}{\sin\theta} = 1 - \cos\Phi \approx \frac{1}{2}\varphi^2 \tag{41}$$

The vertical divergence correction δ_{point} resulting from the use of a point source and a finite crystal of Fig. 16a is calculated by obtaining the mean value of δ:

$$\delta_{point} = \int_{-\varphi_1}^{\varphi_2} \frac{1}{2}\varphi^2 d\varphi \Big/ \int_{-\varphi_1}^{\varphi_2} d\varphi = \frac{1}{6}\left(\varphi_1^2 - \varphi_1\varphi_2 + \varphi_2^2\right) \tag{42}$$

If we consider now a line source, we can use the above result with the substitution of $\varphi_c = \varphi_1 + \varphi_2$ to integrate over the source, using φ_2 as the variable of integration as indicated in Fig.16b. We obtain as the result the vertical divergence correction for a line sample δ_{line}:

$$\delta_{line} = \frac{\displaystyle\int_{\frac{\varphi_c - \varphi_s}{2}}^{\frac{\varphi_c + \varphi_s}{2}} \frac{1}{6}\left[(\varphi_c - \varphi_2)^2 - \varphi_2(\varphi_c - \varphi_2) + \varphi_2^2\right] d\varphi_2}{\displaystyle\int_{\frac{\varphi_c - \varphi_s}{2}}^{\frac{\varphi_c + \varphi_s}{2}} d\varphi_2}$$

$$= \frac{1}{24} \left(\varphi_s^2 + \varphi_c^2\right) \quad , \tag{43}$$

where φ_c is the vertical angle subtended by the crystal of height c as viewed from the sample and φ_s is the vertical angle subtended by the sample of length s as viewed from the crystal.

If the entire line sample should be displaced vertically by a distance d from its true alignment, then the correction for vertical divergence, $\delta_{displaced}$, is

$$\delta_{displaced} = \frac{\displaystyle\int_{\frac{\varphi_c - \varphi_s + 2\varphi_d}{2}}^{\frac{\varphi_c + \varphi_s + 2\varphi_d}{2}} \frac{1}{6}\left[(\varphi_c - \varphi_2)^2 - \varphi_2(\varphi_c - \varphi_2) + \varphi_2^2\right] d\varphi_2}{\displaystyle\int_{\frac{\varphi_c - \varphi_s + 2\varphi_d}{2}}^{\frac{\varphi_c + \varphi_s + 2\varphi_d}{2}} d\varphi_2}$$

$$= \frac{1}{24}\left(\varphi_s^2 + \varphi_c^2\right) + \frac{1}{2}\varphi_d^2 \tag{44}$$

where $\varphi_d = \arctan\left(\frac{d}{\ell}\right)$.

This experiment is not concerned with the absolute wavelength but with the relative wavelength difference between two sources. We are concerned therefore, with two relative changes in the vertical

divergence correction: 1) the change $\Delta (\delta_{line})$ between samples of different length Δ s calculated by differentiating Eq. (43)

$$\Delta (\delta_{line}) = \frac{1}{12} \varphi_s \Delta \varphi_s \text{ , and} \qquad (45)$$

2) the change $\Delta (\delta_{displaced})$ between samples which have been mounted at heights differing slightly by the amount Δ d calculated in a similar manner from Eq. (44)

$$\Delta (\delta_{displaced}) = \varphi_d \Delta \varphi_d \text{ .} \qquad (46)$$

The length s of every sample was 1 ± 1/16 inch. Using these values and Eq. (45), we have $\Delta (\delta_{line}) = \pm 8.2 \times 10^{-7}$. This represents a shift in wavelength $\Delta (\lambda_{line}) = \pm 0.0001$ x-units which is almost small enough to be safely neglected. To make certain, vertical window defining slits (see Fig. 6) were added in front of the lead housing and they were adjusted to just clip the top and bottom of the samples so that as viewed from the crystal, the effective length s was the same for all samples.

From Eq. (46) it is seen that φ_d should be made as small as possible. With the aid of a level (sensitive to a fraction of a second), the crystal turntable axis was adjusted to within 5 seconds of being vertical. The sample table and sample holder were then adjusted so that the center of the sample was to within ± 1/16" of being at the same height as the center of the bent-crystal, thus making d = 0 ± 1/16 inch. A displacement d = 1/16" produced a relative shift in wavelength of 0.00004 x-units. The previously mentioned addition of the vertical

window defining slits further reduces chances of error from this source.

Vertical divergence effects can still enter the isotope shift result through a non-uniformity in the distribution of the sample material within the quartz capillary tube. Visually, the isotope samples appear to be very consistent. But, for purposes of calculation, assume a defective sample in which 10% of the material is concentrated in one lump at one end of the capillary. Then the calculated change in the wavelength relative to a uniformly distributed sample is of the order of 0.00016 x-units. Therefore, the importance of good samples and careful alignment of the spectrometer is recognized.

APPENDIX IV

DETAILS OF THE DATA REDUCTION

A. Step One- Reduction of Cycle Data

The data from each cycle are first reduced independently. These data consist of the number of counts versus spectrometer position for four consecutive sweeps over the line on a given side of the spectrometer. Initially, the data of each sweep are scanned for consistency with the other three sweeps to draw attention to any possible spectrometer or data recording control failures, etc. Passing this test, the counts of the four sweeps are combined into one equivalent sweep by adding the counts for each position. This equivalent line is then fitted by a least-squares program to a Gaussian function:

$$y(x) = P1\{1 + P2\ (x - P4)\} + P3\ e^{-4 \ln (2)\{ \frac{x - P4}{P5} \}^2} \tag{47}$$

in which the independent variable x stands for the x-unit reading and where the five free parameters are:

P1 = background counts

P2 = slope of background

P3 = height of peak above background

P4 = center of peak in x-units

P5 = FWHM of line in x-units

The shape of the observed line results from a fold of the instrumental window with the natural line shape of the x-ray. Although the natural line shape of the x-ray is a Lorentzian function, it is so narrow

(see Fig. 1) relative to the instrumental width that the observed line can be fitted very well with a Gaussian function. This is demonstrated in Fig. 10 which presents the experimental data and the resulting fitted Gaussian curve for a typical cycle.

Although the parameter of interest is the peak-center, P4, the values of the other four fitted parameters are also saved from the least-squares reduction of each cycle as an aid to the interpretation of the data (see Appendix V). Figure 17 presents a plot of the values of the five parameters for each cycle during run HR.

B. Step Two - Reduction of the Run Data

In the second step, the set of peak-center values, P4, from the series of plus and minus cycles yields a set of consecutive wavelength measurements. The measured wavelength corresponds to one-half the difference between a plus-side peak-center measurement P4(+) and a minus-side peak-center measurement P4(-). As can be noted from the lowest plot in Fig. 17 , the results for P4 are not particularly stable. The value for P4 varies with slow long-term drifts which are interrupted by occasional jumps. Described in Appendix V-B are some of the efforts that have been made to isolate the origin and reduce or eliminate these drifts.

The effects of the long-term drifts are cancelled by reducing each P4(-) value with the average of the P4(+) values which precede and follow it:

$$\lambda^{i}_{\text{SINGLE MEASUREMENT}} = \frac{\{P4(+)^{2i-1} + P4(+)^{2i+1}\}/2 - P4(-)^{2i}}{2} \tag{48}$$

where the index i runs from 1 to n to include all (2n + 1) cycles. "SINGLE MEASUREMENT" will be abbreviated by "SM" in the discussion which follows.

The resulting series of wavelength measurements, λ^{i}_{SM}, can be seen by means of the next to lowest plot in Fig. 17 to be considerably more stable than P4. The same scale is used for λ^{i}_{SM} as for P4 in the plot. The effect from the spurious values for λ^{i}_{SM} which occur whenever there is a sudden jump or reversal in trend in P4 must be averaged out by taking a sufficient number of λ^{i}_{SM} measurements. The average of λ^{i}_{SM} for the run, λ_{RUN}, its standard deviation σ_{RUN}, and the standard deviation for a single measurement, σ_{SM}, are formed in the usual way for the n measurements in the run:

$$\lambda_{RUN} = \frac{\sum_{i=1}^{n} \lambda^{i}_{SM}}{n} \tag{49a}$$

$$\sigma_{RUN} = \sqrt{\frac{\sum_{i=1}^{n} (\lambda^{i}_{SM} - \lambda_{RUN})^2}{n(n-1)}} \tag{49b}$$

$$\sigma_{SM} = \sqrt{n}\, \sigma_{RUN} \tag{49c}$$

C. Step Three - Obtaining the Weighted Mean

The final result for the wavelength of each isotope could be

taken as the average of the λ_{RUN} values from all the runs of a given isotope. It is desirable, however, to apply a weighting factor which gives more weight to those particular runs in which jumps in P4 have been less frequent or less severe.

It can be observed from Table VIII in Appendix VI which lists λ_{RUN}, σ_{RUN}, and σ_{SM} of the various runs, that the standard deviations vary from run to run therefore making it worthwhile to apply a weighting factor. We can derive from σ_{SM} the weighting factor we desire if we apply it to the λ_{SM} values instead of the λ_{RUN} values. Therefore, in the last step of the data reduction, we take:

$$\lambda_{FINAL} = \frac{\sum_{i=1}^{N} \lambda_{SM}^{i} \cdot W^{i}}{\sum_{i=1}^{N} W^{i}} \qquad (50)$$

where N is the total number of single measurements taken in all the runs of one isotope combined, and where the weighting factor W^i is

$$W^{i} = \left(\frac{1}{\sigma_{SM}^{i}} \right)^{2} \qquad (51)$$

in which the value for σ_{SM}^{i} corresponds to the σ_{SM} of the run of which λ_{SM}^{i} is a member.

In the usual manner, the standard deviation for the weighted average σ_{FINAL} is:

$$\sigma_{FINAL} = \sqrt{\frac{1}{N-1} \cdot \frac{\sum_{i=1}^{N} (\lambda_{SM}^{i} - \lambda_{FINAL})^{2} \cdot W^{i}}{\sum_{i=1}^{N} W^{i}}} \qquad (52)$$

The final results given in Table IV were computed in this manner.

For comparison, if the unweighted average is taken instead, the final results for all runs of each isotope are:

λ (U-238)	=	125.68056	0.00016 x-units
λ (U-233)	=	125.67829	0.00020 "
Isotope Shift	=	0.00227	0.00026 "

The wavelength values are not appreciably different from the weighted results. But the standard deviation is a little larger because the poorer data received as much weight as the more consistent data did. Therefore, the final results presented in Table IV used the weighted average.

APPENDIX V

SYSTEMATIC ERROR CONSIDERATIONS

Because the isotope shift effect is so small, careful consideration must be given to possible sources of systematic errors in the experiment, either from instrument bias or sample effects. For this reason, the values for the other four parameters resulting from the least squares fit (see Eq. (47)) were plotted versus cycle, (see Fig. 17). In addition, all parameter values were averaged for each run and any variations which appeared between different samples or different runs were studied. Also, the room temperature was observed to an accuracy of ± 0.1 degrees Centigrade and any variations noted.

A) Sample Position Effect

Movements of the sample in either the sideways direction or in the vertical direction are of concern. The former affects the beta-point of the measurement, and the latter can cause sizeable apparent shifts in the wavelength if the instrument is not well aligned. These two effects are now considered in order.

As illustrated in Fig. 9 , the beta-point is the effective zero of the instrument. The spectrometer is operated with the beta-point as close to the actual main dial zero-point as possible, but slight deviations are unavoidable since a sideways displacement of the sample by only 8 microns will shift the beta-point by 0.01 x-units. The experiment was conducted with the majority of the runs having a beta-point of - 0.15 to -0.23 x-units. The effect of variations in

the value of the beta-point should be checked because of the presence of wow in the sine-screw mechanism (see Appendix II-D and the graph in Fig. 4). A plot of the results of the individual runs versus beta-point values shown in Fig. 18 indicates that both the beta-point variation and the wow of the sine-screw mechanism are small enough so that the results have not been systematically affected.

We shall now consider vertical displacement effects. As is discussed in Appendix III-C, should the instrument be poorly aligned, a variation in the height of the mounting of the sample from one run to the next or a non-uniformity in the distribution of the material within the quartz tube of one isotope could make sizeable wavelength shifts. On the other hand, careful alignment of the sample table height relative to the bent-crystal elevation should make vertical divergence effects small since vertical divergence effects are proportional to the square of the displacement from true alignment. These effects should be further reduced by the placement of the vertical window defining slits. Although the alignment was determined optically to be good, it was deemed desirable to confirm it by purposely taking one run with the sample lowered by 5/16". As is shown in the data of Table III, the wavelength measured for this test run is not in disagreement with the other runs. The result confirms that the spectrometer sample table is not misaligned.

B. Changes in the Beta-Point during a Run

As noted in Appendix IV-B, both long-term drifts and occasional sudden jumps in the beta-point occurred during the runs. A considerable

amount of investigation has been made to find the sources of these drifts. The plots of the other parameters from the least-square fits for all the runs (of which Fig. 17 is an example) have been studied for clues or correlations. A search for correlations with temperature, A-C line voltage and time of day has been tried. The drifts seem to be random in nature. There has been no indication of the drift originating from anything other than two general sources:

1. movement of the sample and/or crystal-pivot unit relative to one another, and
2. fine mechanical changes in the spectrometer crystal-pivot unit (see Fig. 5) at such likely points as the thrust bearing, stepping motor, or stepping-motor-to-lead-screw-coupling.

As many steps as possible were taken to control or eliminate these sources of drift during the setting-up of the experiment described in Chapter IV, of which mounting the critical parts on a concrete isolation slab is an example. But it was observed during the thermo-micrometer measurements that physical bending of the slab and transfer of building vibrations still occurred, although to a much reduced extent. It must be realized that a movement of only 1 micron of the sample relative to the crystal 2 meters away can produce a shift of more than 0.001 x-units in the beta-point and that over periods of time, movement from vibration and flexing of this magnitude can be expected. The method of taking fast and frequent sweeps over the lines and performing the measurement many times worked quite well in averaging out random effects. Because it might be expected that some

of the disturbances are related with the time of day, the runs were begun and terminated as much as possible at the same time each day.

C. X-Ray Output Stability

If the x-ray output were to fluctuate in an unfavorable manner so as to give on the average a higher counting rate while the spectrometer is on one side of the peak than while on the other, then the measured wavelength will be shifted. To prevent this, the filament voltage to the x-ray tube was regulated. However, the high voltage on the target is not regulated and can vary with the primary AC line voltage. As a test, the spectrometer was left on the center of the peak and the counting rate monitored. The output stability was good. The experimental procedure of forming a peak from four repeated fast-scans over the x-ray line serves to further average out x-ray output fluctuations.

D. Height and FWHM of the Lines

The results for the other parameters in the least-aquares fit were also averaged for the various runs. The line widths are very nearly the same for the 4 different ten-mil samples showing that the diameters are very well matched:

Sample	*FWHM (x-units)*
First U-233 ten-mil	0.375
Second U-233 ten-mil	0.377
First U-238 ten-mil	0.380
Second U-238 ten-mil	0.379
First U-238 seven-mil	0.310

However, both U-238 samples show greater peak heights than the corresponding U-233 samples. In this one respect the samples for the two isotopes are not well matched as the U-238 capillaries contain more material than the U-233 samples. It would have been desirable to have had the samples matched in every respect, but limited isotope material was available and it was entirely used in making the present samples. Fortunately, wavelength determinations with the bent-crystal spectrometer are not at all sensitive to the source strength except with regard to the size of the error bars one obtains for a given time length of measuring. To compensate for this, the number of U-233 cycles taken was approximately twice that of the U-238 samples. As added assurance, it can be seen that the seven-mil U-238 sample which also has about one-half the material of the ten-mil samples, gave within statistics the same result as the ten mil U-238 samples (see Table III).

E. Background and Slope

The two remaining parameters from the least-squares fit are the background and the slope of the background. The background behaved in a very reasonable manner, being slighly higher for the U-238 than for the U-233 samples because of the greater material in the U-238 samples. The slope likewise tended to be slightly greater for the U-238 samples. It was because the slope of the background might vary with the samples that it was included as one of the five parameters in the least-squares fit so that it would not affect the line center. As a check on this, a plot of the measured wavelength versus the sum of the slope

average for the minus and plus cycles for the various runs of the two isotopes is presented in Fig. 19 . The slope is in units of the fractional change in the background per x-unit. It is seen that as expected, there is no dependence of the measured wavelength on the slope.

APPENDIX VI

ADDITIONAL DATA FOR THE INDIVIDUAL RUNS

We present in Table VIII the average values for the five parameters which resulted for the 19 runs which were performed.

Column 1 Run identification.

Column 2 Sample identification. The entry of the form U-NUMBER-LETTER-NUMBER stands for:
U - uranium
LETTER - A - first quartz capillary
B - second quartz capillary
NUMBER - sample diameter in mils.

Column 3 Number of cycles run consists of. A cycle is four sweeps over the line and requires 1 hr.

Column 4,5,6
λ_{RUN}, σ_{RUN}, and σ_{SM} defined by Eq. (49).

Column 7 Beta point. See Fig. 9.

Column 8,9,10,11
Averages for the four additional parameters. See Eq. (47).

Run HW was conducted with the sample lowered 5/16" from the standard height as a test.

Table VIII

RUN	SAMPLE	CYCLES	λ_{RUN} x-units	σ_{RUN} x-units	σ_{SM} x-units	Beta x-units	BKGD	HEIGHT	SLOPE	FWHM
HD	U233310	22	125.67882	0.00048	0.0015	-C.160	233	292	0.019	0.376
HE	U238310	24	125.68100	0.00033	0.0011	-C.190	263	540	0.024	0.379
HF	U233310	24	125.67906	0.00062	0.0021	-C.203	243	305	0.022	0.378
HG	U238310	24	125.68114	0.00038	0.0013	-C.088	260	504	0.028	0.378
HJ	U233310	25	125.67897	0.00080	0.0027	-C.207	229	272	0.020	0.379
HK	U238310	24	125.68079	0.00034	0.0011	-C.179	258	496	0.025	0.379
HL	U233310	24	125.67820	0.00039	0.0013	-C.214	239	311	0.024	0.373
HM	U233A10	17	125.67923	0.00119	0.0034	-C.321	260	291	0.021	0.378
HN	U233A10	26	125.67793	0.00054	0.0019	-C.195	249	265	0.018	0.375
HO	U233310	23	125.67754	0.00056	0.0019	-C.167	249	304	0.024	0.381
HP	U233A10	32	125.67780	0.00046	0.0018	-C.188	273	298	0.022	0.376
HQ	U233B10	23	125.67870	0.00044	0.0014	-C.147	306	401	0.019	0.376
HR	U238B10	23	125.68006	0.00032	0.0010	-C.215	336	695	0.025	0.379
HS	U233A10	23	125.67818	0.00053	0.0018	-C.187	317	348	0.020	0.373
HT	U238A7	23	125.68048	0.00069	0.0023	-C.085	325	345	0.016	0.310
HU	U233A10	23	125.67738	0.00099	0.0033	-C.182	332	369	0.013	0.373
HW	U238B10	19	125.68034	0.00031	0.0012	-0.185	317	584	0.029	0.380
HX	U238A10	23	125.68044	0.00058	0.0019	-0.027	311	612	0.017	0.380
HY	U238B10	14	125.68044	0.00065	0.0016	-0.185	343	730	0.022	0.379

REFERENCES

1. T.R. Merton, Nature 104, 406 (1919).
2. J.H. Bartlett, Nature 128, 408 (1931).
3. W. Pauli and R.E. Peierls, Phys. Z. 32, 670 (1931).
4. G. Racah, Nature 129, 723 (1932).
5. J.E. Rosenthal and G. Breit, Phys. Rev. 41, 459 (1932).
6. G. Breit, Phys. Rev. 42, 348 (1932).
7. J.E. Mack and H. Arroe, Ann. Rev. Nuclear Sci. 6, 117 (1956).
8. P. Brix and H. Kopfermann, Revs. Modern Phys. 30, 517 (1958).
9. G. Breit, Revs. Modern Phys. 30, 507 (1958).
10. H. Kopfermann, Nuclear Moments (Academic Press Inc., New York, 1958) pp. 167 - 188.
11. A.S. Reiner and L. Wilets, Nuclear Phys. 36, 457 (1962).
12. F.K. Richtmyer and S.W. Barnes, Phys. Rev. 37, 1695 (1931).
13. J.H. Williams, Phys. Rev. 37, 1431 (1931).
14. Frilly, Gokhale, and Valadarès, Compt. rend. 233, 1183 (1951).
15. C.L. Rogosa and C. Schwarz, Phys. Rev. 98, 1 (1955).
16. M.S. Wertheim and G. Igo, Phys. Rev. 92, 1434 (1953).
17. E. Hatch, private communication.
18. J.A. Bearden, X-Ray Wavelengths (A.E.C., Oak Ridge, 1964) p. 9.
19. G.T. Ewan and R.L. Graham "Internal Conversion Studies at Very High Resolution", Alpha-Beta and Gamma-Ray Spectroscopy. (North Holland Pub. Co., Amsterdam, 1965), Vol. 2 p. 971.
20. G. Breit and G.E. Brown, Phys. Rev. 76, 1307 (1949).
21. J.R. Reitz, Phys. Rev. 77, 10 (1950).

22. E.J. Konopinski and M.E. Rose "The Theory of Nuclear β Decay", Alpha-Beta and Gamma-Ray Spectroscopy. (North Holland Pub. Co., Amsterdam, 1965), Vol. 2, p. 1360.

23. E.J. Seppi, H.E. Henrikson, F. Boehm and J.W.M. DuMond, Nucl. Instr. and Meths. 16, 17 (1962).

24. The thermo-micrometer, capable of detecting displacements as small as 5 Å, is under development by Dr. Milton Clauser, Rolling Hills, California.

25. L. Wilets "Isotope Shifts", Encyclopedia of Physics. (Springer Verlag, Berlin, 1958), Vol 38/1, p. 96; also see Table 32 of Ref. 10.

26. D.D. Smith, G.L. Stukenbroeker, and J.R. McNally, Jr., Phys. Rev. 84, 383 (1951).

27. A.R. Striganov and L.A. Korostyleva, JETP 2, 277 (1956).

28. For example, see p. 461 of reference 11, or p. 115 of reference 25.

29. R.J. Hull and H.H. Stroke, Phys. Rev. 122, 1574 (1961).

30. For example, compare reference 11 with reference 25.

31. See p. 181 of reference 10.

32. L. Wilets, D.L. Hill, and K.W. Ford, Phys. Rev. 91, 1488 (1953).

33. A. Bohr and B. Mottelson, Dan. Mat. Fys. Medd. 30, No. 1 (1955).

34. R.E. Bell, S. Bjørnholm, and J.C. Severiens, Mat. Fys. Medd. Dan. Vid. Selsk. 32, No. 12 (1960).

35. J.O. Newton, Nuclear Phys. 3, 345 (1957).

36. J.O. Newton, Nuclear Phys. 5, 218 (1957).

37. E. Feenberg, Phys. Rev. 59, 149 (1941).

38. See p. 110 of reference 25.

39. D.S. Falk and L. Wilets, Phys. Rev. 124, 1895 (1961).

40. See page 112 of reference 25.

41. G. Breit, G.B. Arfken and Clendennin, Phys. Rev. 78, 390 (1950).

42. L.R.B. Elton, Nuclear Phys. 8, 396 (1958).

43. F.A. Babushkin, Optics and Spectroscopy 15, 393 (1963).

44. Model SS250 - 1004 manufactured by Superior Electric Co, Bristol, Conn.

45. See Fig. 3 of reference 23.

46. O. Beckman, P. Bergvall, and B. Axelsson, Arkiv Fysik 14, 419 (1958).

Figure 1

Natural line-width of K x-rays as a function of Z. Through use of Eqs. (1) and (2), the measured values of the natural line-widths in eV[19] are converted to line-widths expressed in x-units. The spectrometer instrumental width for a 10-mil sample is indicated by the horizontal line.

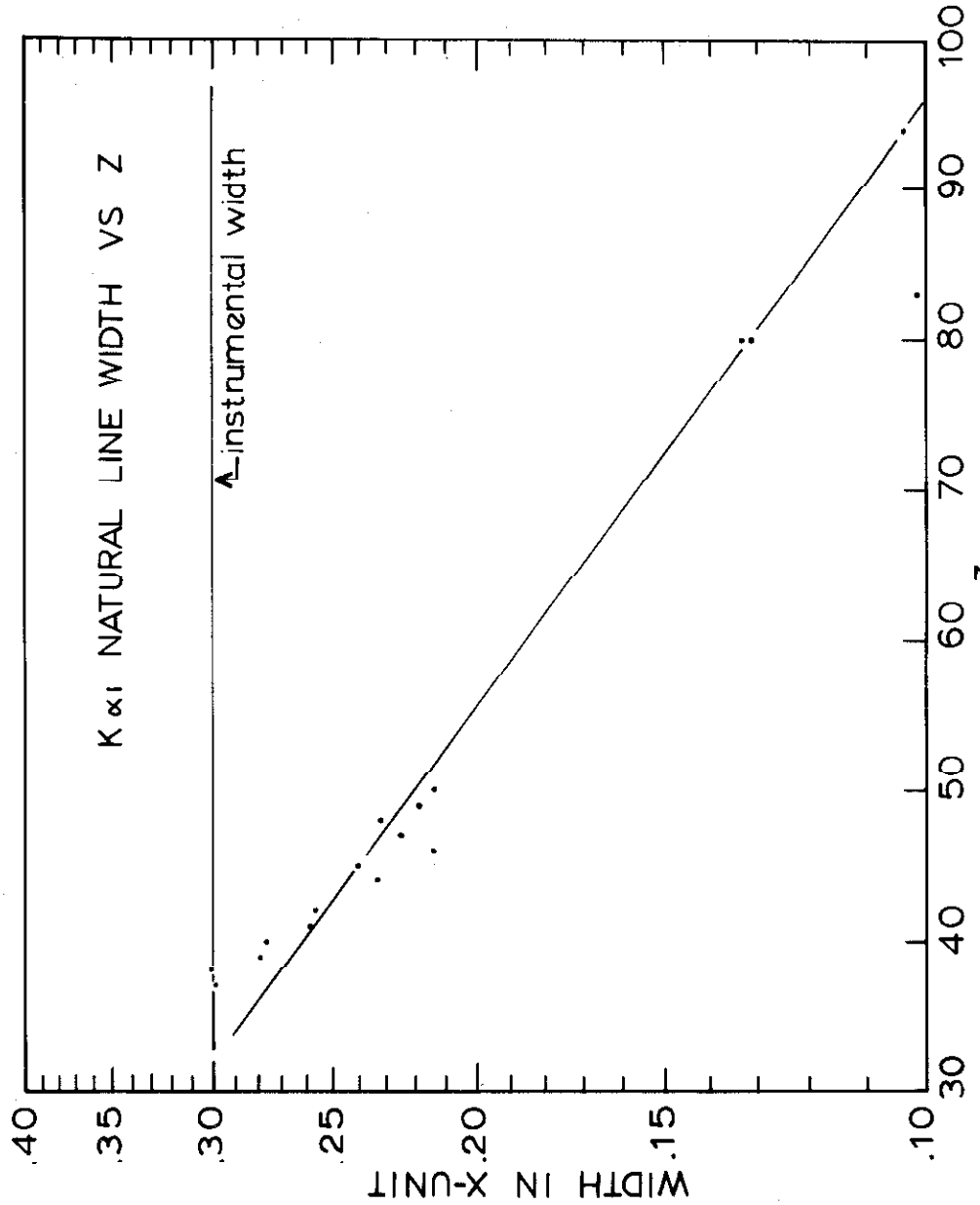
K α1 NATURAL LINE WIDTH VS Z
instrumental width
WIDTH IN X-UNIT
Z
.40
.35
.30
.25
.20
.15
.10
30
40
50
60
70
80
90
100

Figure 1.

Figure 2

Log plot of Wertheim and Igo's first order perturbation calculation result. The values for the shift of the $1s_{\frac{1}{2}}$ electron for $_{42}Mo$, $_{82}Pb$, and $_{92}U$ were calculated using a top-slice model of the nucleus[16]. The size of the shift expressed in energy units exhibits a Z^6 dependence.

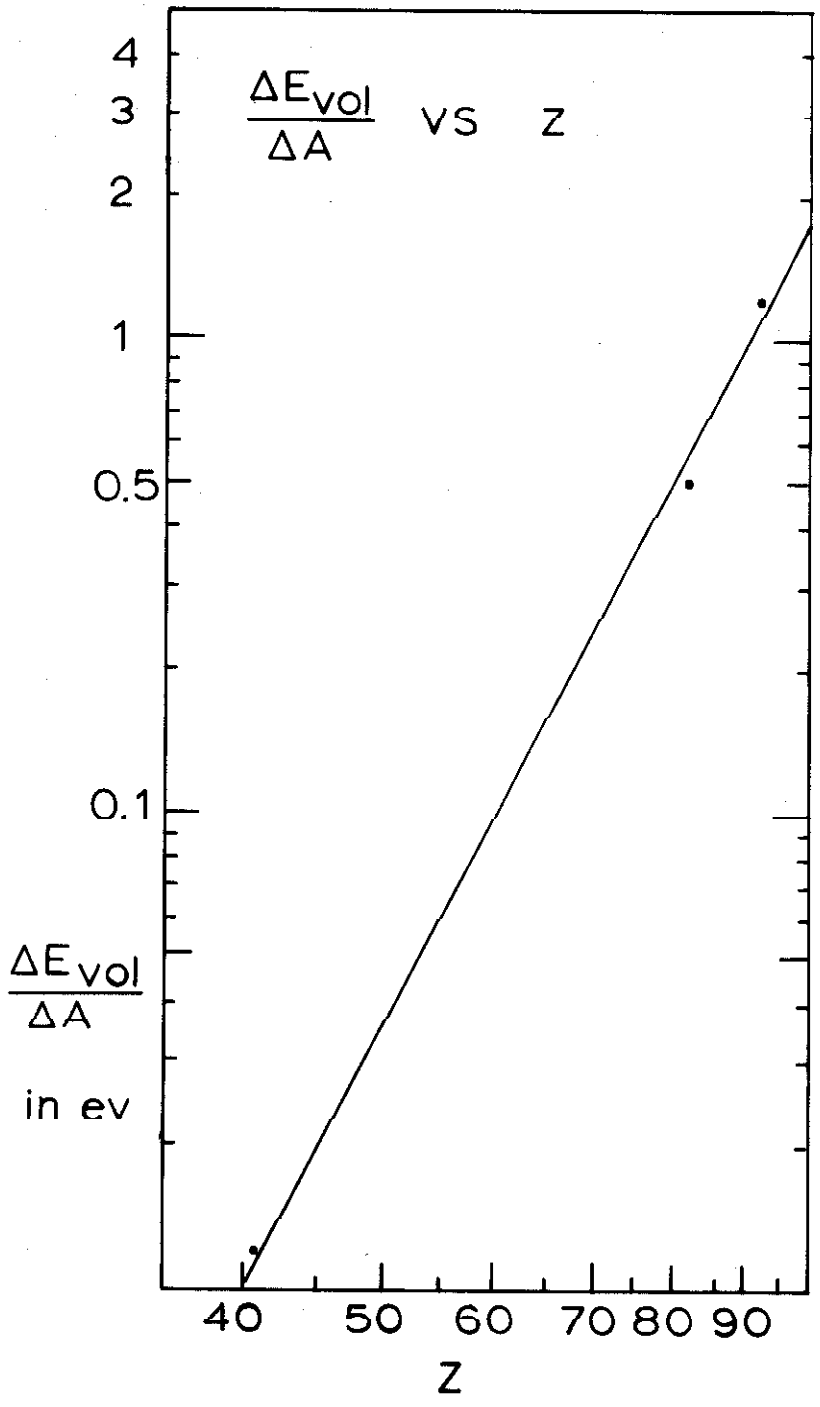
$\frac{\Delta E_{vol}}{\Delta A}$ vs Z
4
3
2
1
0.5
0.1
$\frac{\Delta E_{vol}}{\Delta A}$
in ev
40
50
60
70
80
90
Z

Figure 2

Figure 3

Schematic of layout used to detect the isotope shift. The sample is placed at the focus of the bent-crystal spectrometer. The x-ray tube is operated well above the K_{abs} edge to produce fluorescent x-rays in the sample.

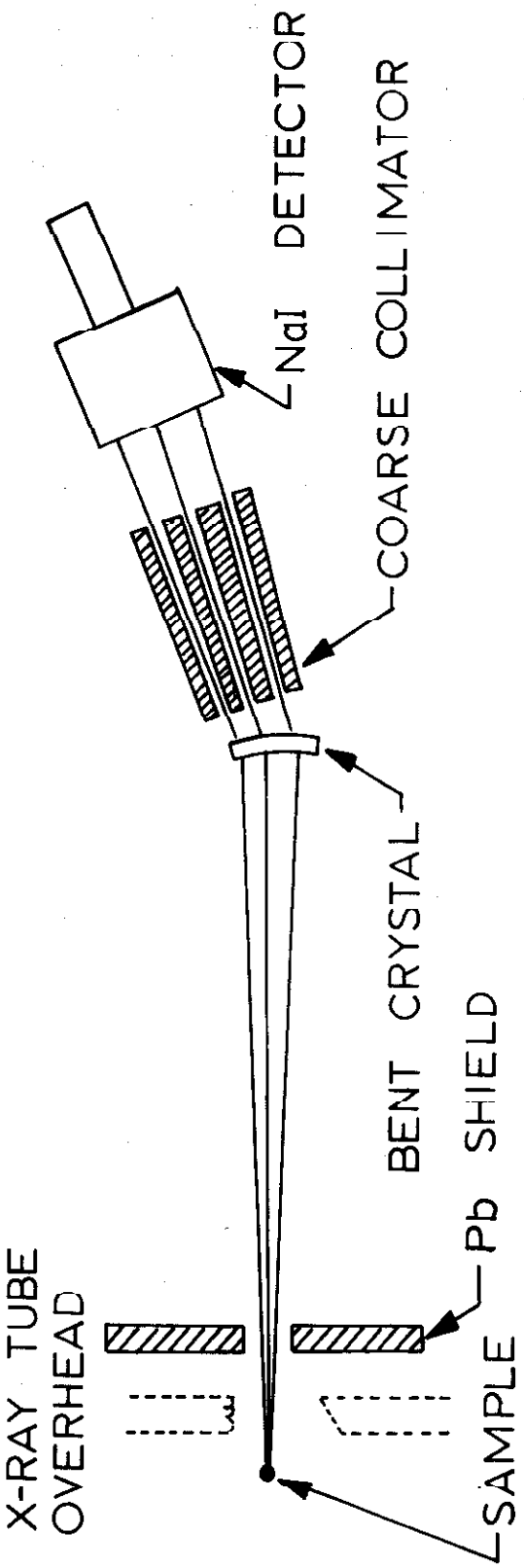
X-RAY TUBE
OVERHEAD
SAMPLE
Pb SHIELD
BENT CRYSTAL
COARSE COLLIMATOR
NaI DETECTOR

Figure 3.

Figure 4

Deviation of the spectrometer mechanism from linearity. Through the use of the thermo-micrometers, small defects in the spectrometer sine-screw mechanism were detected. The "Before" plot is one of many taken before defects in the end plate and thrust bearing were corrected. It exhibits the repetition of the deviations with every revolution (2 x-units). The greatly improved "After" plot still exhibits defects such as wow, but they are not serious. The isotope shift corresponds to 0.2 seconds.

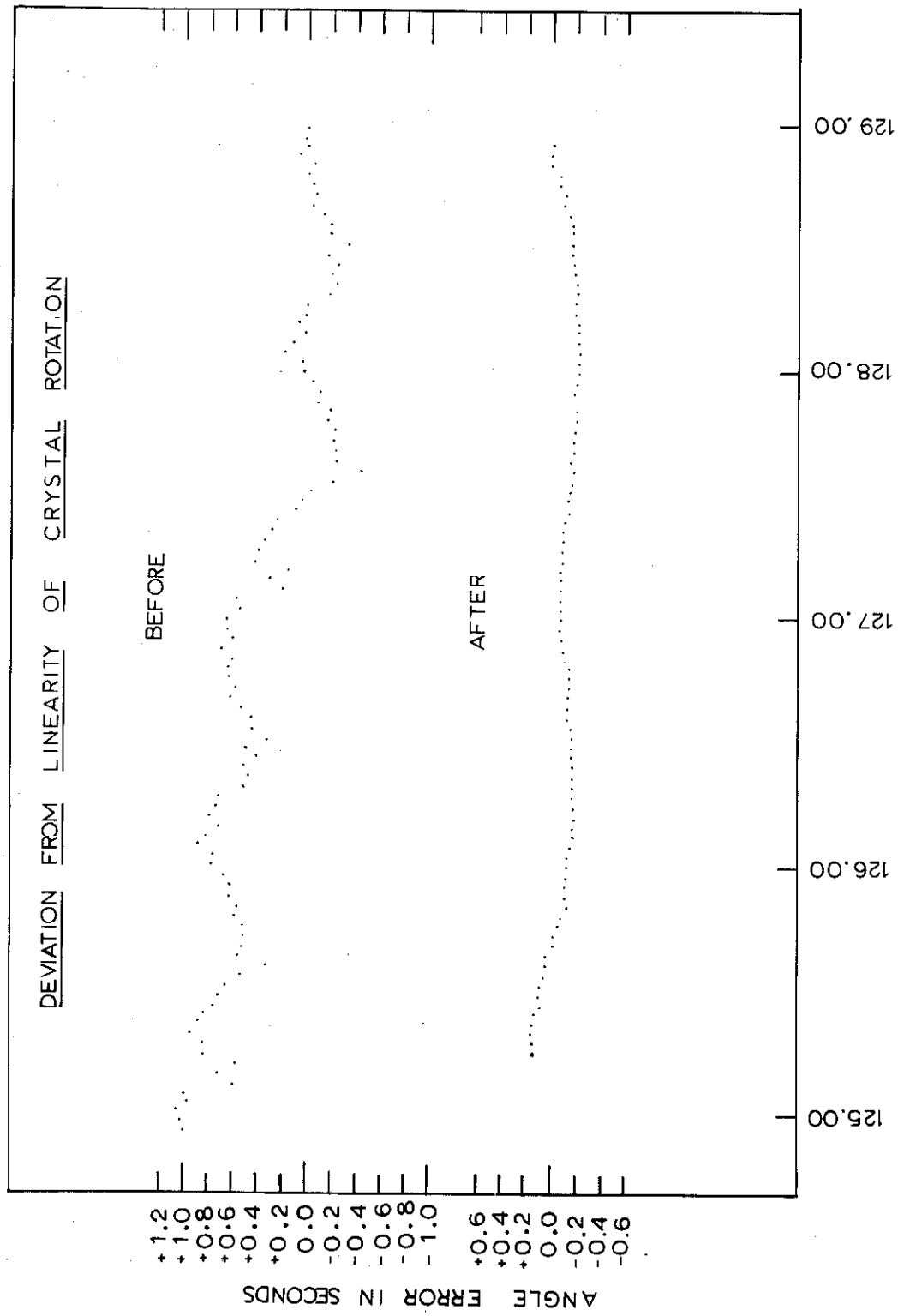
DEVIATION FROM LINEARITY OF CRYSTAL ROTATION
BEFORE
AFTER
ANGLE ERROR IN SECONDS
+1.2
+1.0
+0.8
+0.6
+0.4
+0.2
0.0
-0.2
-0.4
-0.6
-0.8
-1.0
+0.6
+0.4
+0.2
0.0
-0.2
-0.4
-0.6
125.00
126.00
127.00
128.00
129.00
SPECTROMETER POSITION IN X-UNITS

Figure 4

Figure 5.

Detailed line drawing of the experimental set-up. Some of the critical points in the experiment are displayed. The necessary shielding is not shown.

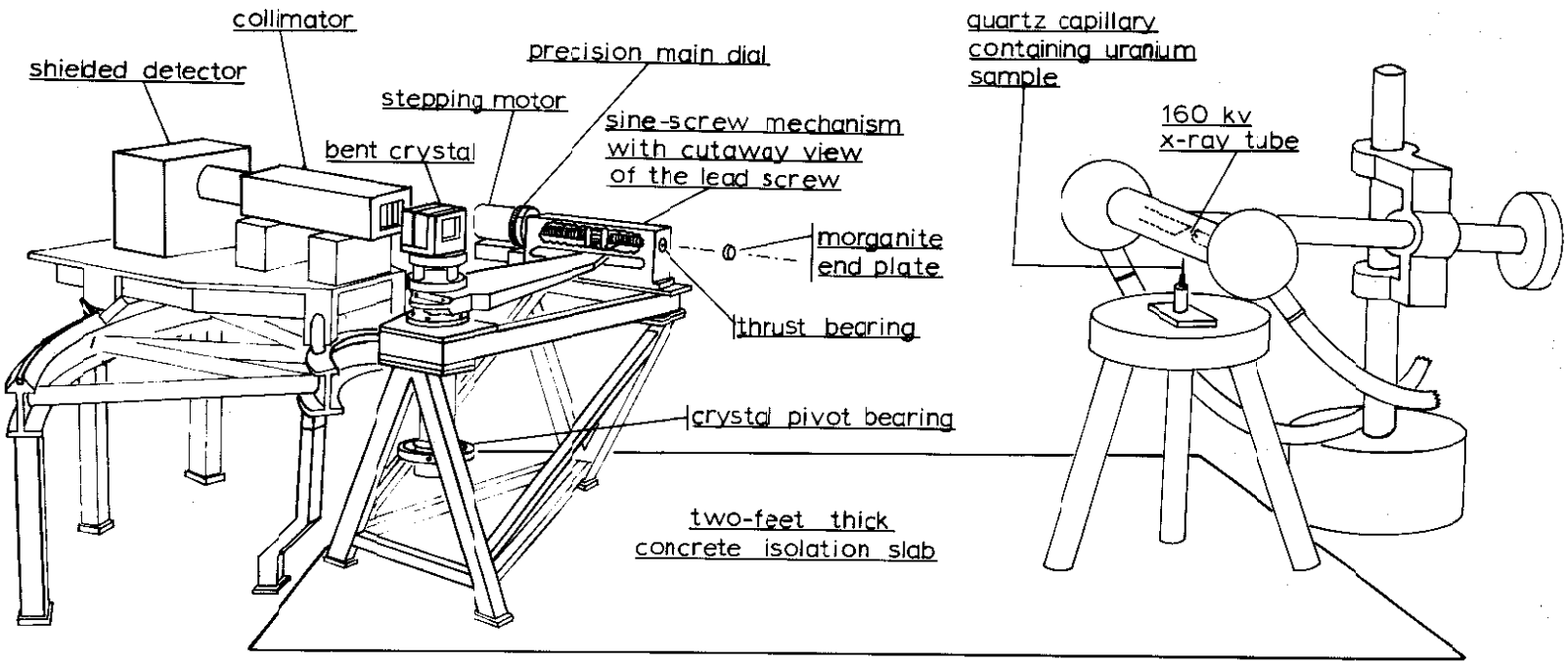
collimator
shielded detector
precision main dial
stepping motor
bent crystal
sine-screw mechanism
with cutaway view
of the lead screw
quartz capillary
containing uranium
sample
160 kv
x-ray tube
morganite
end plate
thrust bearing
crystal pivot bearing
two-feet thick
concrete isolation slab
DETECTOR CARRIAGE
CRYSTAL PIVOT
SAMPLE TABLE
X-RAY UNIT

Figure 5

Figure 6.

Top view of experiment showing method of shielding used. The parts identified are:

A. Backstop shield

B. Lead shielding box

C. X-ray tube

D. Sample

E. Lead plate with hole which defines the vertical window. As viewed from bent-crystal, the window in E just clips the top and bottom of the sample.

F. Lead plate with hole which defines the horizontal window.

G. Lead plate to shield regions towards which the collimator is aimed.

H. Bent-crystal

I. Coarse collimator

J,K Respective positions of the detector for plus and minus scans of the line.

TOP VIEW OF EXPERIMENTAL SETUP
TO SHOW SHIELDING AND SYMMETRY

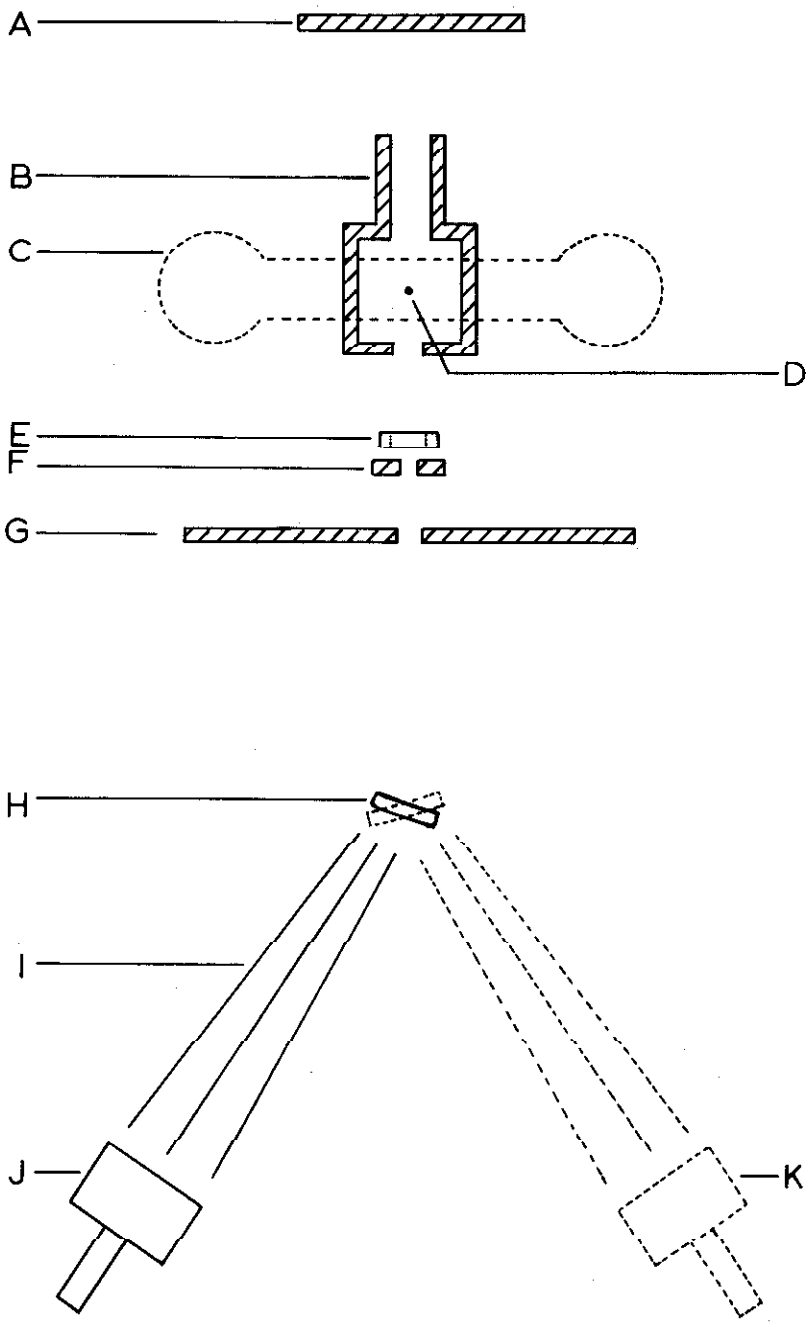

Figure 6.

Figure 7

View of the sample holder.

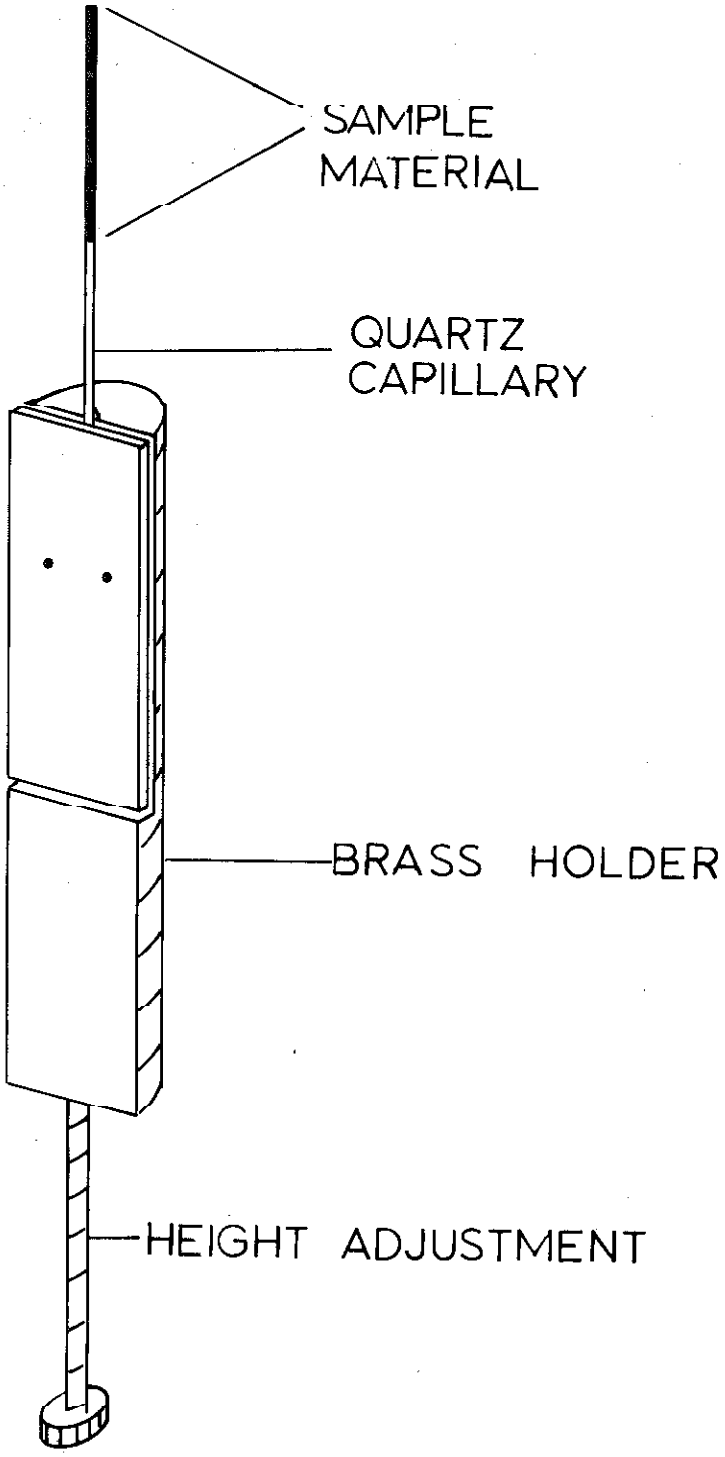
SAMPLE
MATERIAL
QUARTZ
CAPILLARY
BRASS HOLDER
HEIGHT ADJUSTMENT

Figure 7.

Figure 8

General scan in the region of the uranium $K_{\alpha 1}$ x-ray.

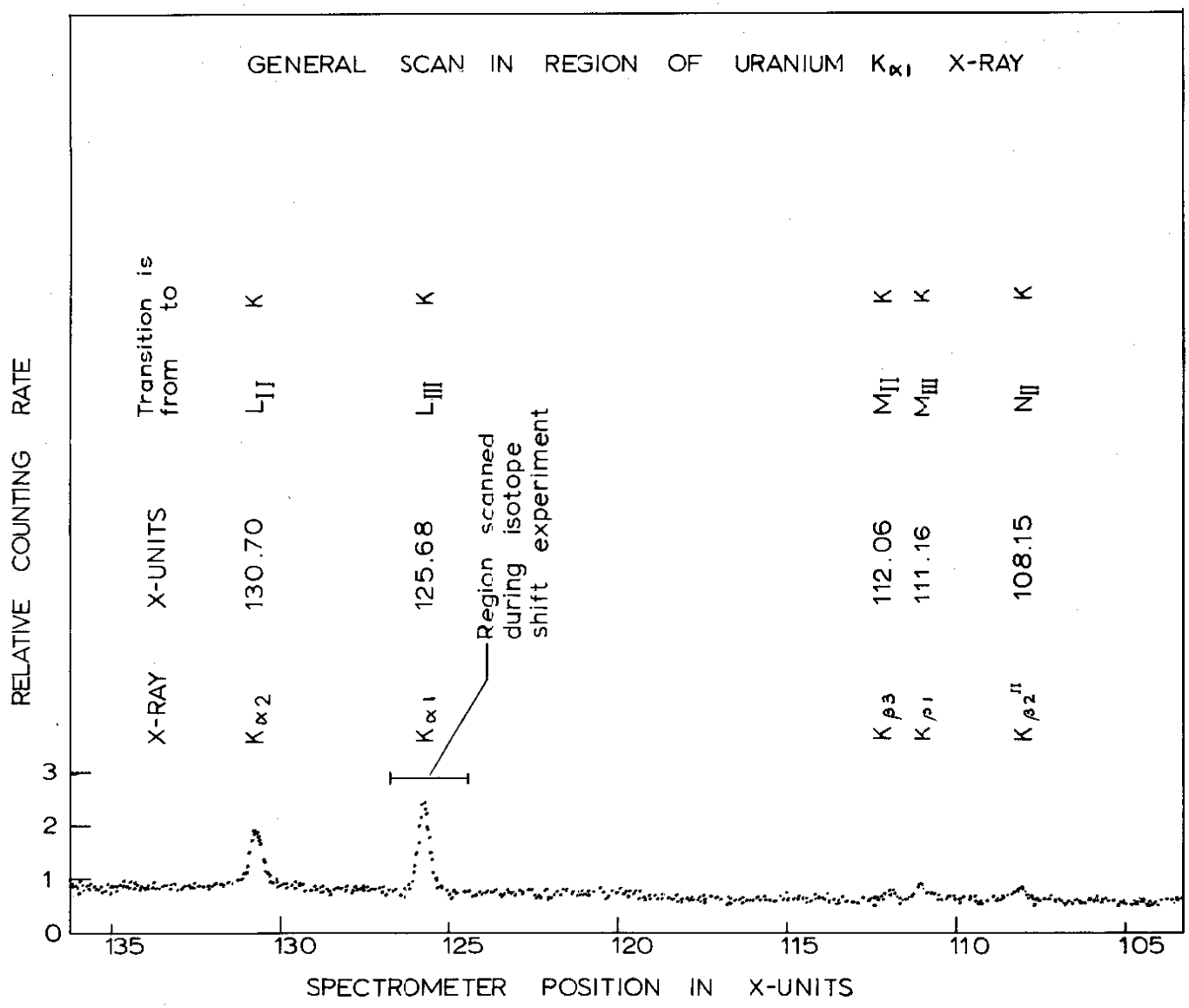
GENERAL SCAN IN REGION OF URANIUM $K_{\alpha 1}$ X-RAY
RELATIVE COUNTING RATE
X-RAY
X-UNITS
Transition is from to
$K_{\alpha 2}$ 130.70 L_{II} K
$K_{\alpha 1}$ 125.68 L_{III} K
Region scanned during isotope shift experiment
$K_{\beta 3}$ 112.06 M_{II} K
$K_{\beta 1}$ 111.16 M_{III} K
$K_{\beta 2}^{II}$ 108.15 N_{II} K
0
1
2
3
135
130
125
120
115
110
105
SPECTROMETER POSITION IN X-UNITS

Figure 8

Figure 9

Illustration of plus and minus scans. The $K_{\alpha 1}$ line center on the plus and minus side are 125.465 and -125.895 x-units respectively. Taking one-half the difference, the measured $K_{\alpha 1}$ wavelength is 125.680 x-units. The zero of the instrument (referred to as the beta point) is -0.215 x-units. The use of a coarse collimator results in the central peak being very broad.

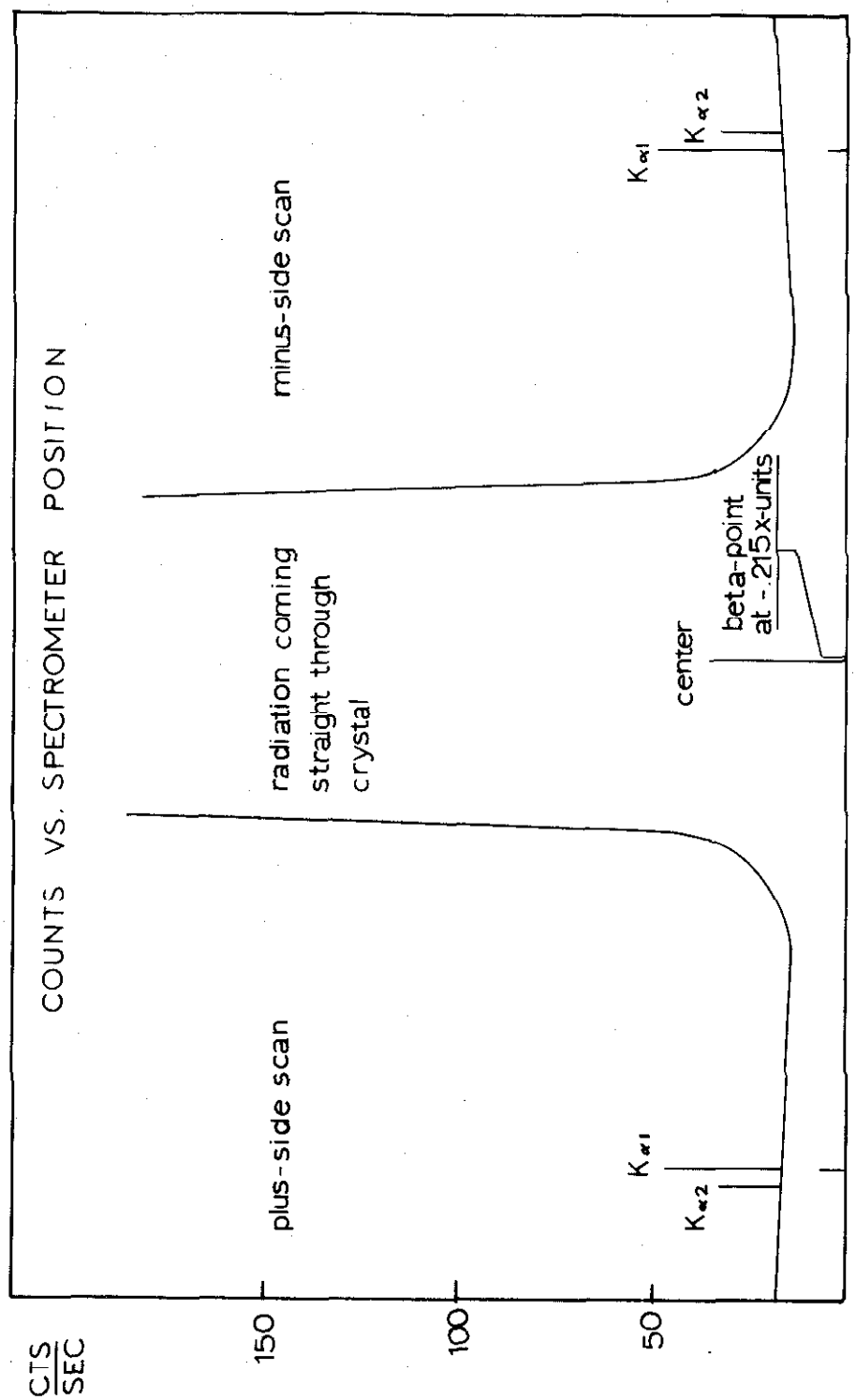
COUNTS VS. SPECTROMETER POSITION
CTS/SEC
150
100
50
plus-side scan
radiation coming straight through crystal
minus-side scan
center
beta-point at -.215 x-units
$K_{\alpha 1}$
$K_{\alpha 2}$
$K_{\alpha 1}$
$K_{\alpha 2}$
+125.465
0
-125.895
SPECTROMETER POSITION IN X-UNITS

Figure 9

Figure 10

Least-squares fit to the $K_{\alpha 1}$ line. The observed $K_{\alpha 1}$ line is fitted very well by the Gaussian function of Eq. (47).

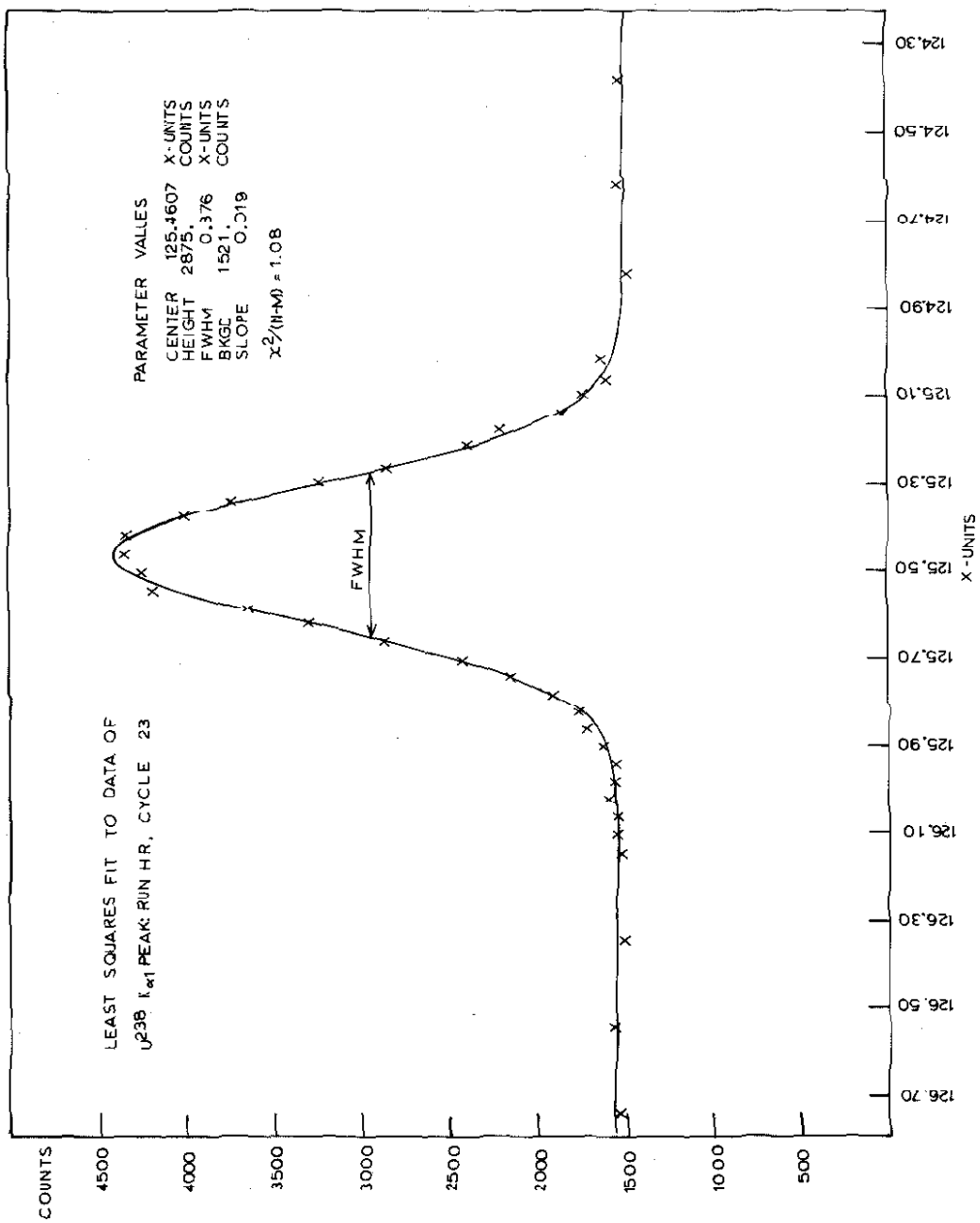
LEAST SQUARES FIT TO DATA OF
U238 Kα1 PEAK: RUN HR, CYCLE 23
PARAMETER VALUES
CENTER 125.4607 X-UNITS
HEIGHT 2875. COUNTS
FWHM 0.376 X-UNITS
BKGD 1521. COUNTS
SLOPE 0.019
χ²/(N-M) = 1.08
FWHM
COUNTS
4500
4000
3500
3000
2500
2000
1500
1000
500
126.70
126.50
126.30
126.10
125.90
125.70
125.50
125.30
125.10
124.90
124.70
124.50
124.30
X-UNITS

Figure 10

Figure 11a

Isotope structure observed in the uranium 4244.372 Å line. The even-odd staggering effect is quite marked. The $\Delta A = 2$ spacing is very regular. Data is taken from reference 26.

Figure 11b

Comparison of isotope shifts in adjacent elements. From the relative isotope positions of mercury (Z = 80) and thallium (Z = 81), it is seen that the isotope shift is quite dependent on neutron number but relatively independent of whether Z is even or odd. Data is taken from references 30 and 31. The dashed lines indicate that the A = 200 and A = 201 isotopes of Hg and Th were used for horizontal alignment.

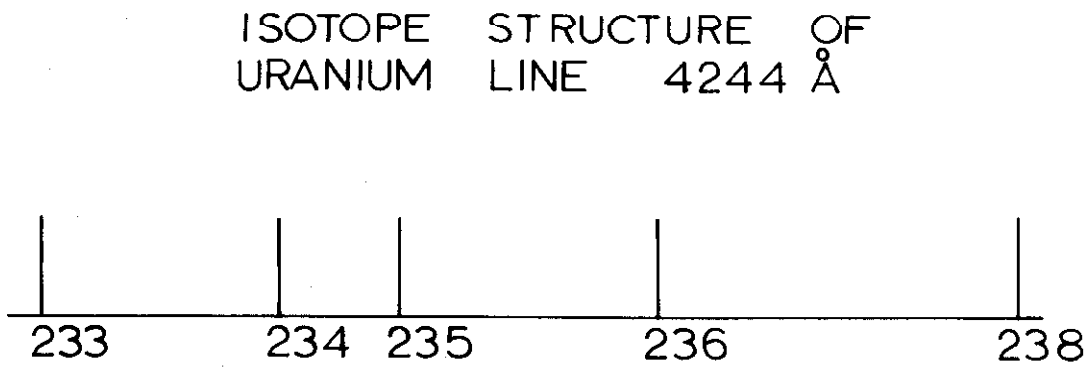

Figure 11a

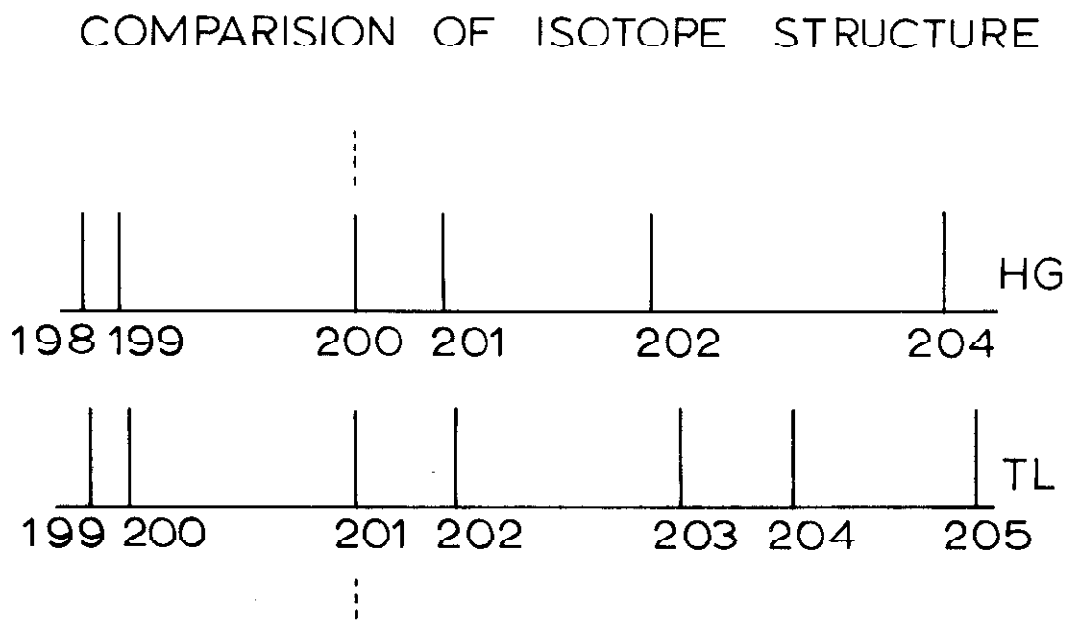

Figure 11b

Figure 12

Observed optical isotope structure compared with the structure predicted by the deformation data for uranium. The optical isotope structure presented at the top of the figure shows much greater regularity than the structure predicted from the experimental values for Q_0 of the uranium isotopes shown at the bottom. It is concluded that the deformation varies smoothly with A for uranium. This figure is based on values given in Table V.

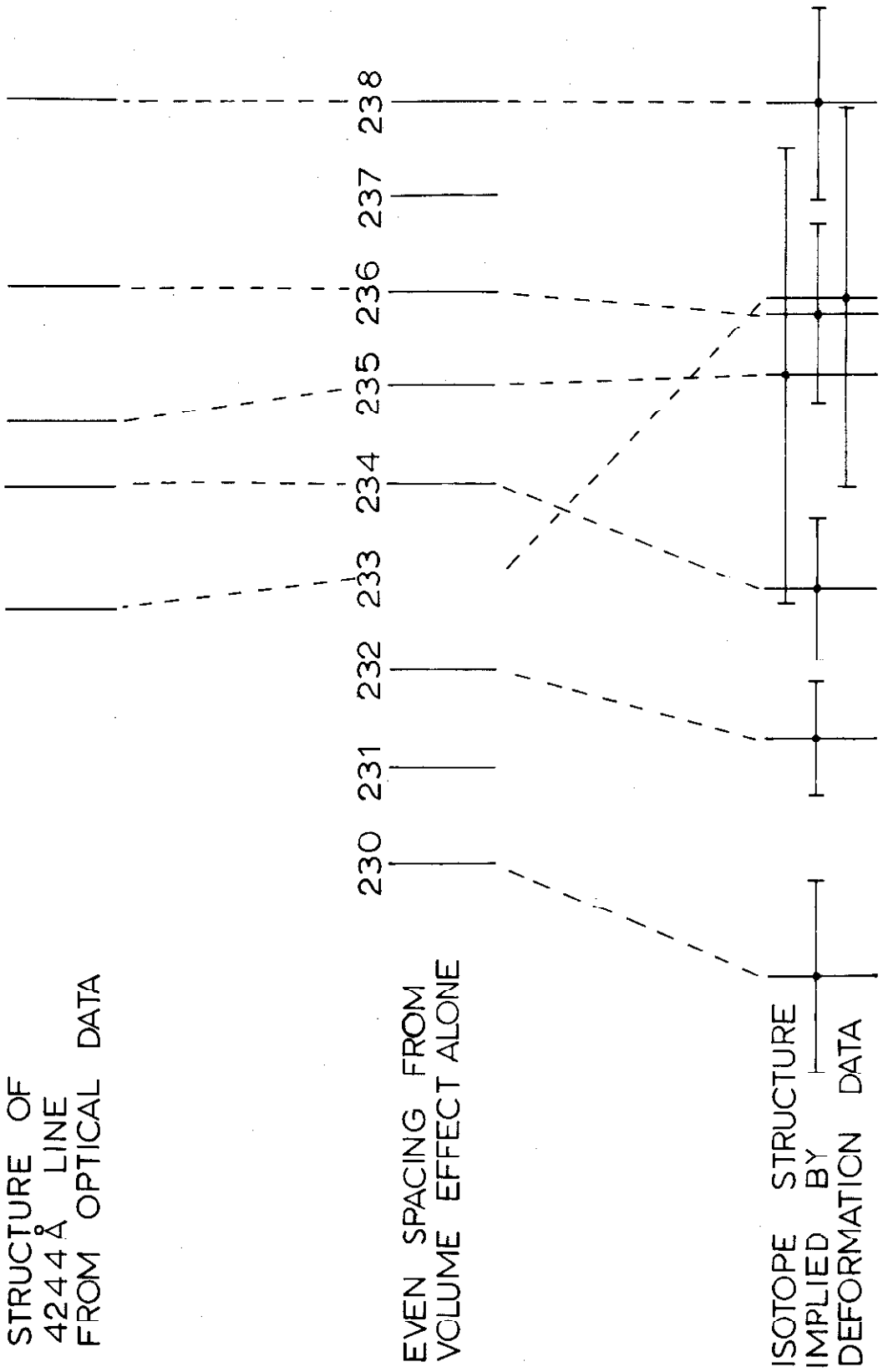
STRUCTURE OF
4244 Å LINE
FROM OPTICAL DATA
EVEN SPACING FROM
VOLUME EFFECT ALONE
ISOTOPE STRUCTURE
IMPLIED BY
DEFORMATION DATA
230
231
232
233
234
235
236
237
238

Figure 12

Figure 13

Experimental values for the intrinsic quadrupole moment Q_0 of the uranium isotopes. The experimental values displayed are taken from references given in Table V. The optical isotope shift data strongly indicates that Q_0 varies smoothly with A for the uranium isotopes (see Fig. 12). Hence, a straight line has been drawn which best fits the intrinsic quadrupole moment data. The dashed lines indicate the change in the value of Q_0 necessary to produce the even-odd staggering observed in Fig. 11a.

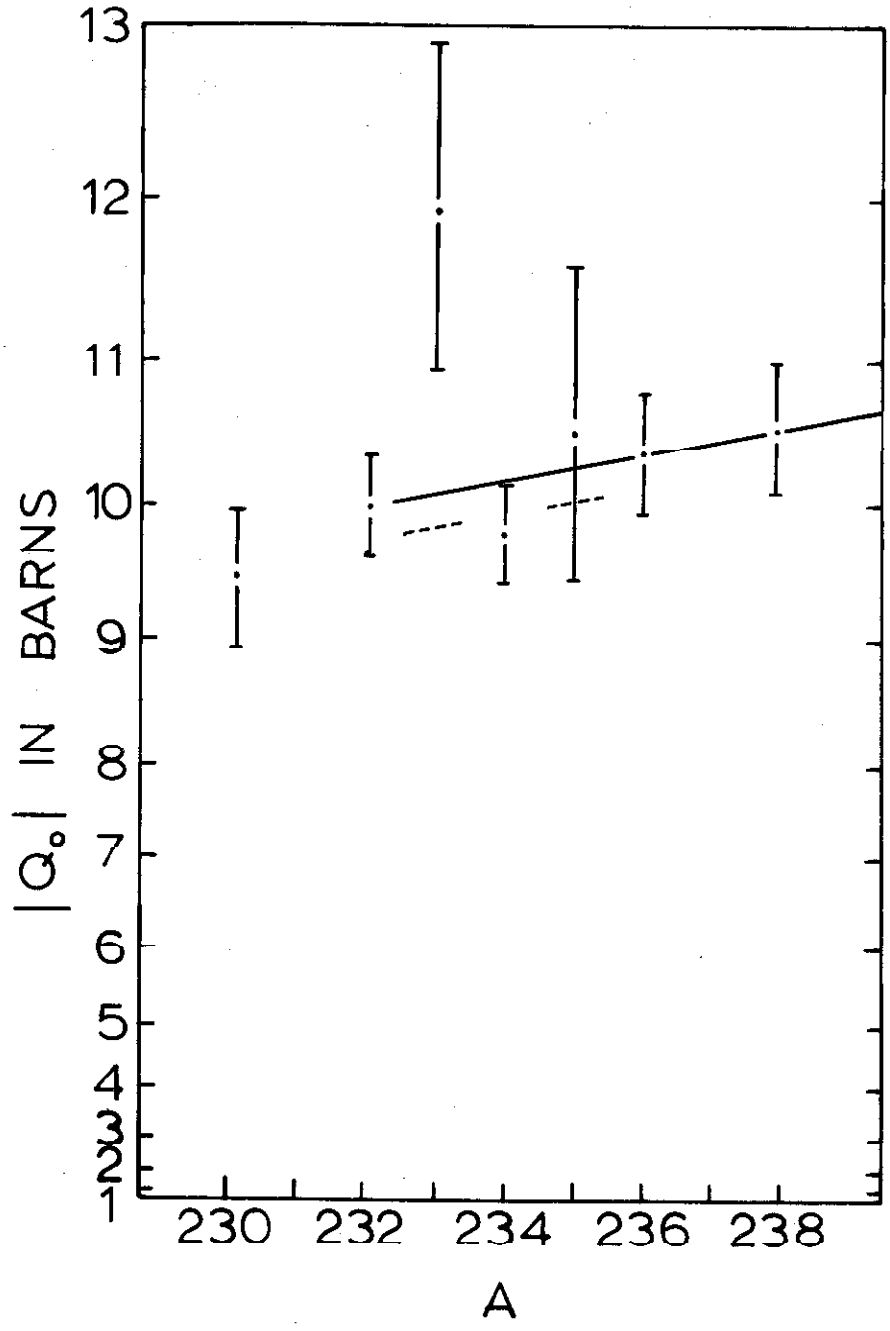

Figure 13

Figure 14

Predicted isotope shifts for the $K_{\alpha 1}$ x-ray. The predicted isotope shift of the $K_{\alpha 1}$ x-ray (based on the spherical, uniformly charged, incompressible model of the nucleus) is represented by the curved line. Predictions including deformation effects are indicated by the dots. The error limit achieved in the present experiment (shown by the horizontal line) indicates that the isotope shift of many isotope pairs can be studied with the bent-crystal spectrometer. This graph is based on predictions made in reference 43.

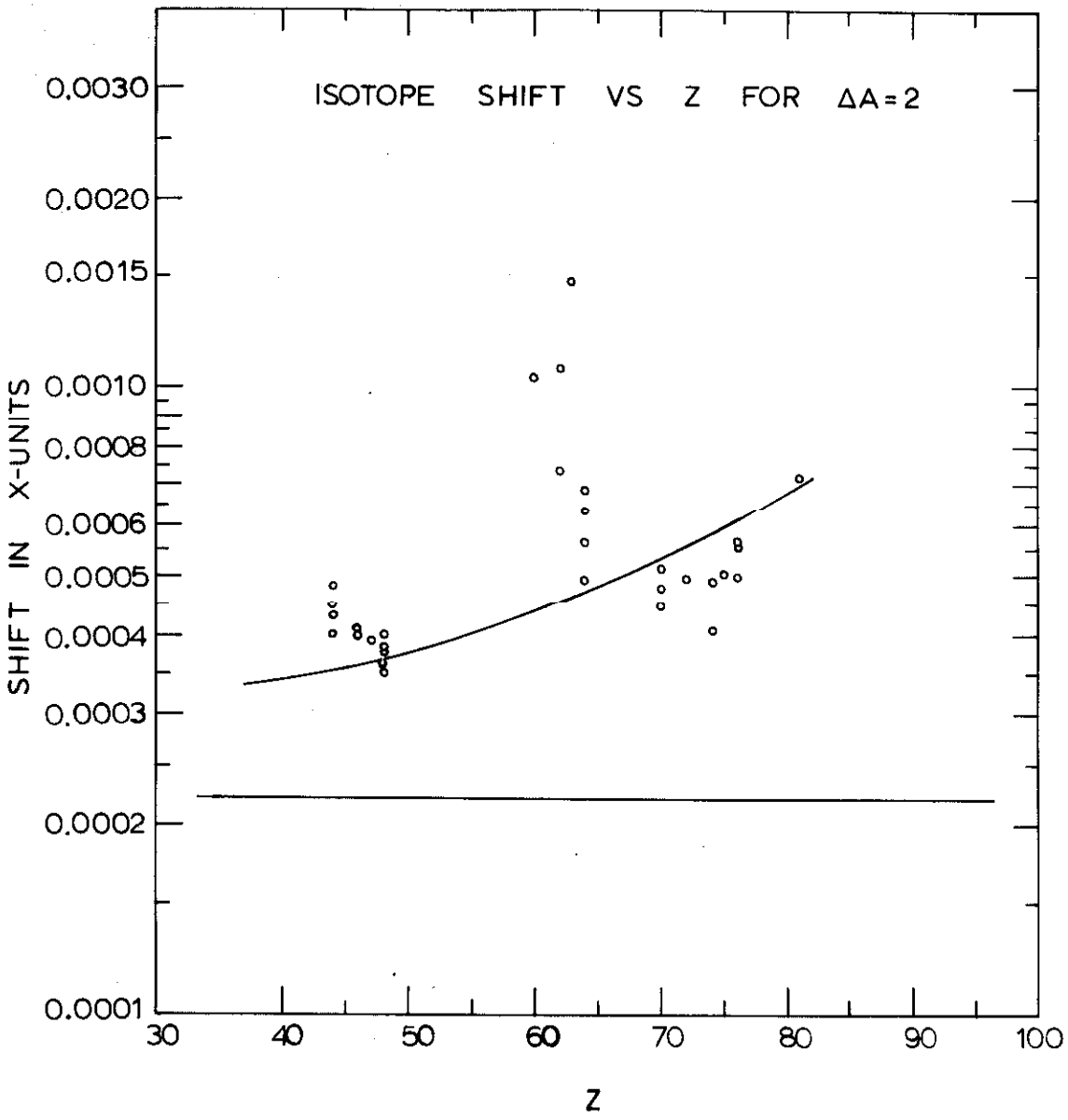
ISOTOPE SHIFT VS Z FOR ΔA=2
SHIFT IN X-UNITS
0.0030
0.0020
0.0015
0.0010
0.0008
0.0006
0.0005
0.0004
0.0003
0.0002
0.0001
30
40
50
60
70
80
90
100
Z

Figure 14

Figure 15

Line drawing of the sine-mechanism. Of interest is the calibration cam (sometimes referred to as the correction cam). It allows for the correction of accumulated errors in the lead-screw by means of advancing or retarding the rotation of the bronze split nut. To eliminate the possibility of its introducing small systematic errors into the isotope shift measurement, its action was defeated. Therefore, absolute wavelength results for an individual isotope in this experiment may contain a systematic error, but it cancels in the isotope shift determination.

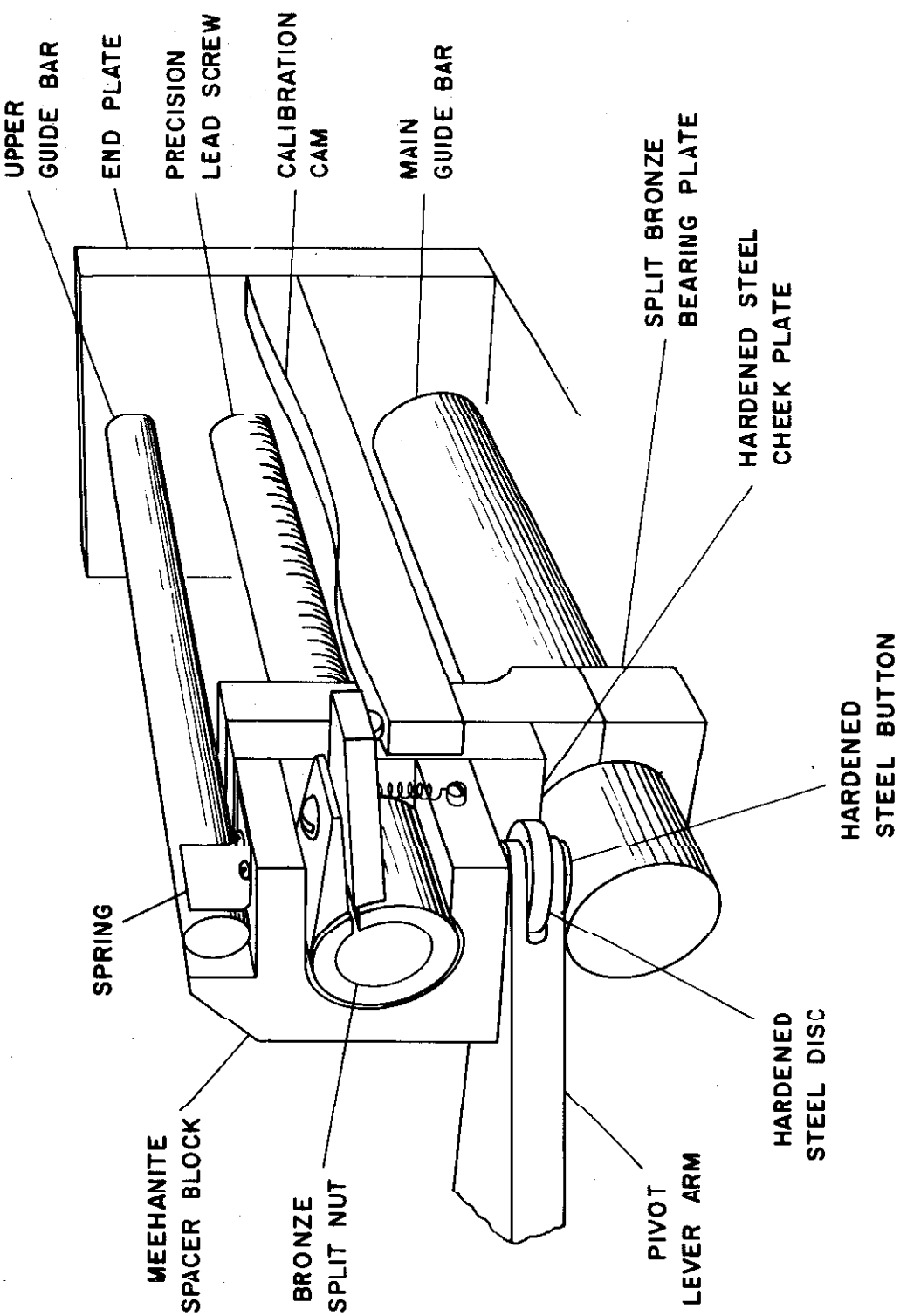
UPPER GUIDE BAR
END PLATE
PRECISION LEAD SCREW
CALIBRATION CAM
MAIN GUIDE BAR
SPLIT BRONZE BEARING PLATE
HARDENED STEEL CHEEK PLATE
HARDENED STEEL BUTTON
SPRING
MEEHANITE SPACER BLOCK
BRONZE SPLIT NUT
HARDENED STEEL DISC
PIVOT LEVER ARM

Figure 15

Figure 16a

Geometry used for the point sample and finite crystal in the vertical divergence correction calculation.

Figure 16b

Geometry used for the finite sample and finite crystal in the vertical divergence correction calculation.

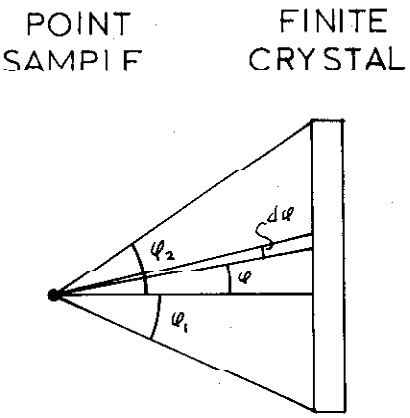

Figure 16a

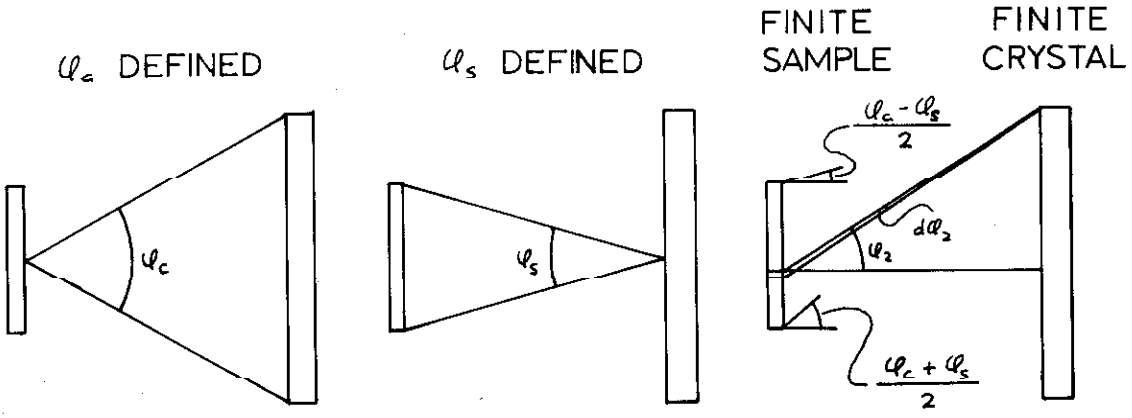

Figure 16b

Figure 17

Parameter plot for a typical run. The values of the five parameters resulting from the least-squares fit of Eq. (47) to the cycle data is shown for run HR. The bottom plot reveals a drift in the value of the instrument beta-point. The method of data reduction used results in a smoother plot for the wavelength determinations λ_{SM} (SM = SINGLE MEASUREMENT in the text). Correlations in the changes of the other parameters with λ_{SM} values have not been observed.

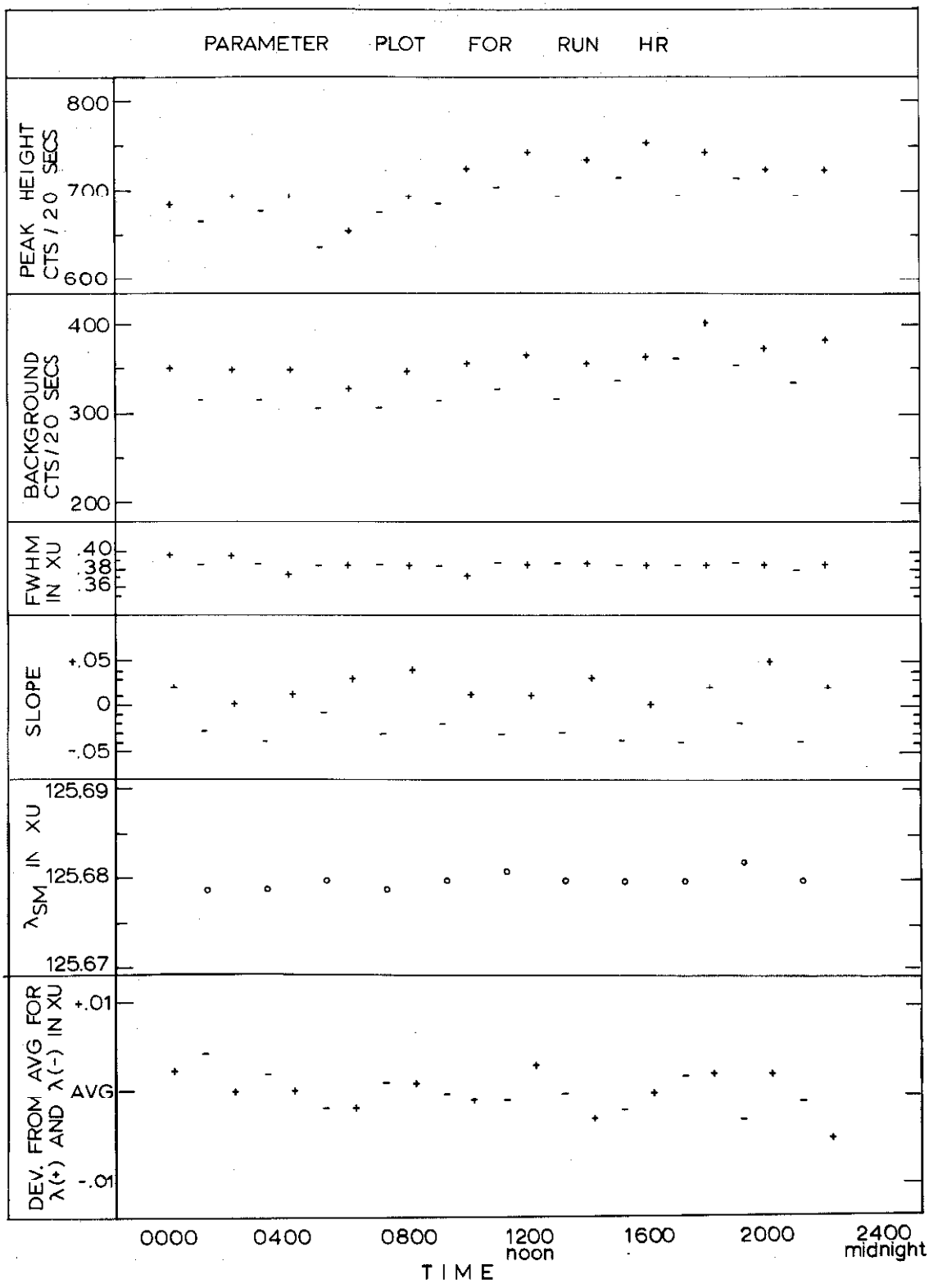
PARAMETER PLOT FOR RUN HR
PEAK HEIGHT CTS / 20 SECS
800
700
600
BACKGROUND CTS / 20 SECS
400
300
200
FWHM IN XU
.40
.38
.36
SLOPE
+.05
0
-.05
λ_{SM} IN XU
125.69
125.68
125.67
DEV. FROM AVG FOR λ(+) AND λ(-) IN XU
+.01
AVG
-.01
0000
0400
0800
1200
noon
1600
2000
2400
midnight
TIME

Figure 17

Figure 18

Wavelength versus sample position. Due to difficulty in preserving the same experimental conditions from run to run, the beta-point of the spectrometer varies. This plot shows that the measured wavelength does not show any dependence on the beta point.

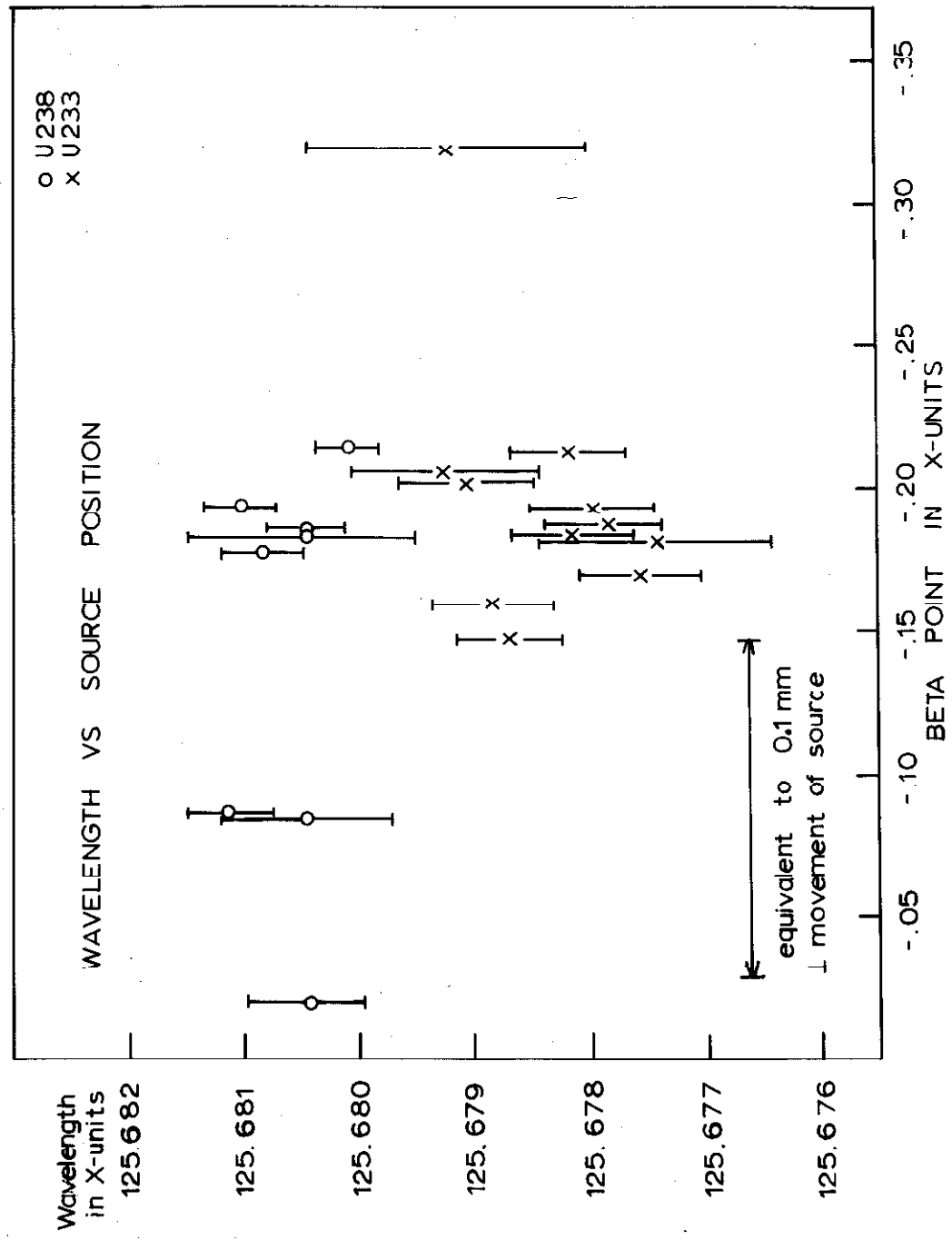
o U238
x U233
WAVELENGTH VS SOURCE POSITION
Wavelength in X-units
125.682
125.681
125.680
125.679
125.678
125.677
125.676
-.05
-.10
-.15
-.20
-.25
-.30
-.35
BETA POINT IN X-UNITS
equivalent to 0.1 mm
⊥ movement of source

Figure 18

Figure 19

Wavelength versus slope of background. The slope varies from run to run and from isotope to isotope. The results appear to be independent of the value for the slope.

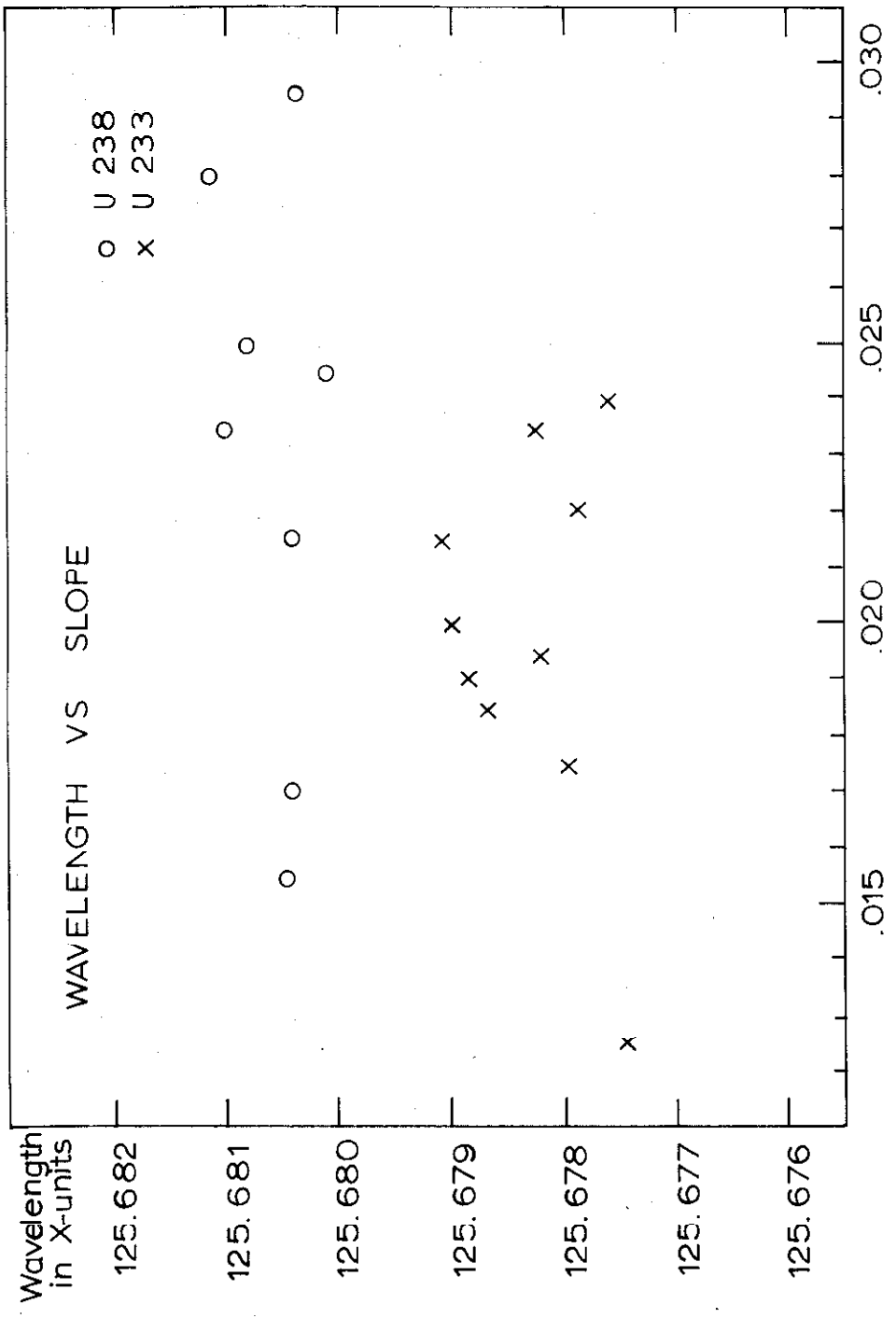
WAVELENGTH VS SLOPE
o U 238
x U 233
Wavelength in X-units
125.682
125.681
125.680
125.679
125.678
125.677
125.676
.015
.020
.025
.030
SLOPE OF BACKGROUND

Figure 19